

Master thesis

EFFECTS OF LEPTO-QUARKS AND
SCALAR GLUONS ON B -MESON
OBSERVABLES



Julius-Maximilians-Universität Würzburg

submitted by

Peter Meinzinger

6th June 2018

Supervisor: Prof. Dr. Werner Porod
Second assessor: Prof. Dr. Raimund Ströhmer

Contents

1. Introduction	1
1.1. Historical overview	1
1.2. Motivation by current progresses	2
2. Preliminaries	5
2.1. Operator Product Expansion	5
2.2. Calculus to \mathcal{R}_K and \mathcal{R}_{K^*}	6
2.3. Standard Model coefficient for $\mathcal{R}_{D^{(*)}}$	7
3. Model basics	9
3.1. The new gauge group	9
3.2. Fermionic sector	10
3.2.1. Gauge eigenstates	10
3.2.2. The fermions' masses	11
3.3. Scalar sector	13
3.3.1. Scalars' spectrum	13
3.3.2. Scalar potential	14
3.3.3. Mixing	15
3.3.4. Transformation into mass eigenstates	16
3.3.5. Fixing the neutral Higgs mass	18
3.4. Gauge bosons	19
4. Phenomenological considerations	21
4.1. New graphs	21
4.2. The mixing matrix of the scalar leptoquarks	24
4.3. Relevant NP calculations	25
4.3.1. Contribution of the scalar gluon G^+ to $b \rightarrow s \gamma$	26
4.3.2. Tree-level contribution for $\mathcal{R}_{D^{(*)}}$	26
4.3.3. Tree-level contribution for $\mathcal{R}_{K^{(*)}}$	27
5. Results	29
5.1. The setup	29
5.2. Scan over m_A	30
5.3. Input for Y_2 and Y_3	31
5.4. Results on $\mathcal{R}_{D^{(*)}}$	33
5.5. Scans over $\tan \beta$ and $m_{R'_{(2)}}$	33
5.6. Scans over the angles' space	35

Contents

6. Conclusion and Outlook	43
A. The SU(4) generators	47
B. Fierz transformation	49
C. The Lagrangian, expanded and after EWSB	51
D. Wilson coefficients	53
D.1. $b \rightarrow s\gamma$	53
D.2. $b \rightarrow sl_i^+ l_i^-$	53
D.2.1. Tensor operator	53
D.2.2. Scalar operators	54
D.2.3. Vector operators	55
D.2.4. Conversion to standard basis	55
D.3. $\bar{b} \rightarrow \bar{c}l_i^+ \nu_\alpha$	56
D.3.1. Scalar operators	56
D.3.2. Vector operators	57
E. Plots	59

Abstract

In this work the model proposed by Fileviez Perez and Wise [1] was examined, especially in face of deviations from the Standard Model in the observables $\mathcal{R}_{K^{(*)}}$ and $\mathcal{R}_{D^{(*)}}$. In a first step the mass structure was analysed and determined, that indeed two out of four leptoquarks might be light. One of these representations, $R_2^{2/3}$ is known to be able to explain these deviations.

Regarding $\mathcal{R}_{D^{(*)}}$, it was seen that the couplings have to be chosen small to avoid violations of experimental data of lepton flavour violating observables. In consequence the Wilson coefficient does not suffice to produce an acceptable deviation from the Standard Model prediction.

In principle $\mathcal{R}_{K^{(*)}}$ can be explained with the effects from $R_2^{2/3}$, bounds from lepton flavour violating decays and leptonic meson decays were violated, though. The biggest restrictions come from the processes $\mu^- \rightarrow e^- e^+ e^-$ and $K_L^0 \rightarrow e^\pm \mu^\mp$. In both cases the effects result through the coupling Y_4 , which is the same as in the Wilson coefficient to $\mathcal{R}_{K^{(*)}}$.

Zusammenfassung

In dieser Arbeit wurde das Modell von Fileviez Perez und Wise [1] untersucht, vor allem in Anbetracht aktueller Abweichungen der Observablen $\mathcal{R}_{K^{(*)}}$ und $\mathcal{R}_{D^{(*)}}$ von den Standard-Modell-Vorhersagen. Zunächst wurde dazu die Massenstruktur bestimmt und festgestellt, dass zwei der vier skalaren Leptoquarks leicht sein können. Eine der beiden Repräsentationen, $R_2^{2/3}$, kann bekanntermaßen Abweichung an den Observablen erzeugen.

Im Falle von $\mathcal{R}_{D^{(*)}}$ wurde jedoch festgestellt, dass die Kopplungen nicht groß genug gewählt werden können, um Abweichungen vom Standard-Modell zu erzeugen ohne leptonische Observablen zu verletzen, vor allem $\mu \rightarrow e\gamma$.

Prinzipiell ist es andererseits möglich, $\mathcal{R}_{K^{(*)}}$ mithilfe von $R_2^{2/3}$ zu erklären, jedoch hat sich auch hier gezeigt, dass experimentelle Einschränkungen von Lepton-Flavour verletzenden Observablen und leptonischen Mesonzerfällen verletzt werden. Die Einschränkungen kamen vor allem durch die Prozesse $\mu^- \rightarrow e^- e^+ e^-$ und $K_L^0 \rightarrow e^\pm \mu^\mp$. Problematisch ist vor allem, dass die Effekte in beiden Fällen durch dieselbe Kopplung Y_4 , die auch die Abweichung zu $\mathcal{R}_{K^{(*)}}$ kontrolliert, verursacht werden.

1. Introduction

1.1. Historical overview

Starting with the development of the Quantum Theory in the 1920s, the understanding of physical nature got a strong boost and an appealing framework. The fundamental difference of the behaviour of quantum particles from what was known until then, combined with special relativity, eventually led to the Quantum Field theory [2]. Step by step, it was discovered that nature consists of more than the particles which had been known until then, namely the electron, proton and photon. One of the ground-breaking experiments was the proof that the proton and the neutron are not even elementary particles, but are built by constituents, the so-called quarks [3, 4]. A huge field of new physics to discover had been opened up.

Since the 1970s, the Standard Model (SM) has been a highly successful model, predicting – in combination with measured data – the existence of the charm [5] and top quark [6] and the Higgs boson [7, 8]. Within collider experiments and measurements of decays of hadrons and elementary particles it has been possible to establish the SM up to an astonishingly high precision [9]. In spite of this, there have been several drawbacks that could not be handled within the model, ever since. First of all, neutrinos are naively expected to have zero mass which is in contrast to their tiny but existing mass that is proved by observation of neutrino oscillations. Another motivation is the fact that it was possible to unify the electromagnetic and the weak interactions into the gauge group $SU(2) \otimes U(1)$. Nevertheless, it is expected that these should again unify with the strong force on a higher scale, described then by a so-called Grand Unified Theory (GUT). Therefore the search for a more precise and complete description of the elementary particles is continuing.

Among the models proposed, there are several which presume an interaction between leptons and quarks via the so-called lepto-quarks (LQ). Their significant property is that they would be able to transform leptons to quarks and vice versa. These models also lead to a more satisfying description of the fundamental interactions, due to the leptons being embedded as the fourth-color particles.

This idea was first presented by Pati and Salam [10], using a $SU(4)_C$ gauge symmetry. The energy scale of their model was too high to be tested within the possible collider experiments, though. Since then, many (phenomenological) studies have been done [11–18], most of them trying to extend the SM by single leptoquarks. A common approach is to consider general groups, e.g. $SO(10)$ or $SU(5)$, which contain the SM gauge group as a subgroup.

The motivation in the above mentioned broader context is – as mentioned – the

1. Introduction

unification of the gauge couplings and the generation of neutrino masses, but a complete theory might also provide an explanation for dark matter.

1.2. Motivation by current progresses

The ever-growing accuracy of the collider experiments has enabled physicists to widen the spectrum of observed quantities, among them rare B meson decays. Processes like $B \rightarrow X_s \gamma$ are suppressed in the SM by the Glashow-Iliopoulos-Maiani mechanism [19, 20]. They are sensitive to new contributions, though [21]. Furthermore, for the case of semi-leptonic decays, they provide a good test of lepton flavour universality (LFU). Many haven't shown any deviation from SM predictions like the mentioned $B \rightarrow X_s \gamma$. Others like the Lepton Flavour Violating (LFV) $\mu \rightarrow e \gamma$ are not present in the SM, at all, and also have not been observed yet.

The $\mathcal{R}_{D^{(*)}}$ measurement

In 2012, however, there were measurements by the BaBar collaboration of the charged-current semi-leptonic observables called \mathcal{R}_D and \mathcal{R}_{D^*} , respectively defined as

$$\mathcal{R}_{D^{(*)}} = \frac{\text{BR}(\bar{B} \rightarrow D^{(*)} \tau \bar{\nu})}{\text{BR}(\bar{B} \rightarrow D^{(*)} l \bar{\nu})}, \quad l = e, \mu, \quad (1.1)$$

which reported a deviation from the SM predictions by 3.5σ [22]. The measurements have repeatedly been confirmed by the BaBar and Belle experiments [23–26] as well as the LHCb collaboration [27, 28] for \mathcal{R}_{D^*} . The latest averaged data state the ratios to be [29]

$$\begin{aligned} \mathcal{R}_D &= 0.407 \pm 0.046 \text{ and} \\ \mathcal{R}_{D^*} &= 0.304 \pm 0.015, \end{aligned} \quad (1.2)$$

where the systematic and statistical errors have been summed in quadrature. This is a strong hint towards a possible LFU violation, which is not inherent in the SM. The predictions are [30, 31]

$$\begin{aligned} \mathcal{R}_D^{\text{SM}} &= 0.300 \pm 0.008 \\ \mathcal{R}_{D^*}^{\text{SM}} &= 0.252 \pm 0.003, \end{aligned} \quad (1.3)$$

Considering the measurements' correlation, these ratios have now a deviation of 4.1σ compared to the SM prediction [29]. This discrepancy is a surprise due to the present tree-level contribution via W boson in the SM [19].

The $\mathcal{R}_{K^{(*)}}$ measurement

A few years after this first anomaly, another two were reported again in two similar B meson decay by the LHCb collaboration [32]. The considered processes were the decays into a (excited) Kaon and two leptons and the observables are defined by

$$\mathcal{R}_{K^{(*)}} = \frac{\text{BR}(\bar{B} \rightarrow K^{(*)} \mu^+ \mu^-)}{\text{BR}(\bar{B} \rightarrow K^{(*)} e^+ e^-)}. \quad (1.4)$$

This is especially interesting because the decay is particularly sensitive to New Physics in the coefficients of $\mathcal{O}_7^{(l)}$, $\mathcal{O}_9^{(l)}$, and $\mathcal{O}_{10}^{(l)}$ [33, 34] (See also chapter 4.3.3 for a definition). The experimental values – with combined errors as before – are [32, 35]

$$\begin{aligned} \mathcal{R}_K &= 0.745 \pm 0.097 \\ \mathcal{R}_{K^*} &= 0.69 \pm 0.12 \end{aligned} \quad (1.5)$$

for the dilepton invariant mass squared bin $1 < q^2 < 6 \text{ GeV}^2$.

All these detections tend to prove the violation of lepton flavour universality and are used to exclude several models. Leptoquark models are naturally of big interest as they are included in the processes at tree-level.

Can a new model give the explanation?

In 2013, Fileviez Perez and Wise [1] proposed a model which linked to the idea of Pati and Salam, but with a much more promising approach. Above all, this model was expected to induce effects at much lower scales and does not suffer from magnetic monopoles. It contains several new physical bosons, eleven scalars and two vectorials, each coupling to every fermion generation.

The subject of the presented thesis is to test whether this model explains the anomalies of low-energy observables from the latest data of collider experiments. For this purpose, the model was implemented in SARAH [36–39] to generate the necessary files for the spectrum generator SPheno [40, 41]. Subsequently, the mass hierarchy was examined and the parameter space was confined using experimental bounds.

Therefore, this work is organized as follows:

Firstly, the operator product expansion is explained and general considerations on $\mathcal{R}_{K^{(*)}}$ and $\mathcal{R}_{D^{(*)}}$ are presented. Then, in chapter 3 the model is examined, determining the structure of the particle spectrum and the mass hierarchy. In chapter 4 phenomenological analyses are done, regarding relevant graphs, the leptoquark mixing and the new contributions to decays that might explain or violate experimental data. Eventually, the numeric results are discussed in chapter 5 before the work gets summarized in chapter 6.

In the following the quantum numbers of the particles are denoted as $(a, b, c)_{LQ}$ for the transformation under $SU(4)_C, SU(2)_L$ and $U(1)_R$, respectively, and in analogy

1. Introduction

as $(k, l, m)_{\text{SM}}$ for the SM gauge group $SU(3) \otimes SU(2)_L \otimes U(1)_Y$. All spinors are considered to be two-component.

2. Preliminaries

This chapter is here to present the necessary formalism, discuss observed anomalies among the meson observables as well as some remarks about the their calculation.

2.1. Operator Product Expansion

In order to make theoretical predictions for hadron decays, as happening in collider experiments, the help of the so-called Operator Product Expansion (OPE) is necessary. The typical energies of the hadrons of $O(1 \text{ GeV})$ are much lower than the Electro-Weak Symmetry Break (EWSB) scale, e.g. energies of $O(m_{W,Z})$. Thus, the OPE was introduced as a solution to this multi-scale problem [42, 43]. It provides an effective low energy theory to describe the hadronic decays [19, 33, 44].

The basic idea is to treat the interaction as point-like as illustrated in 2.1. Therefore, one introduces an effective Hamiltonian defined as

$$\mathcal{H}_{\text{eff}} = \sum_i C_i(\mu) \cdot \mathcal{O}_i(\mu) . \quad (2.1)$$

and, calculating a matrix element \mathcal{M} using this effective theory, the formula becomes

$$\mathcal{M}(A \rightarrow B) = \langle A | \mathcal{H}_{\text{eff}} | B \rangle = \sum_i C_i(\mu) \cdot \langle A | \mathcal{O}_i(\mu) | B \rangle \quad (2.2)$$

for arbitrary states A and B . The variable μ denotes the renormalization scale, whose dependence has to cancel in the overall expression. Normally it is chosen to be equal to the b-quark mass. The physics is split into two parts: the operators \mathcal{O}

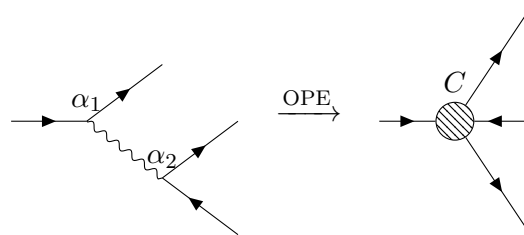


Figure 2.1.: Visual explanation of the Operator Product Expansion: the heavy physics gets encoded into "couplings" C and the light physics into an effective vertex \mathcal{O} .

2. Preliminaries

contain only the light SM fields, i.e. the quarks except the top quark, the leptons as well as photons and gluons. The so-called Wilson coefficients C carry now the short-distance physics, so contributions from heavy particles. Figuratively, one can see these two parts as couplings C to vertices \mathcal{O} [19, 33, 44].

The virtue of this expansion in regard to New Physics (NP) is that one has only to compute new contributions to the Wilson coefficients and – only if necessary – extend the set of operators.

2.2. Calculus to \mathcal{R}_K and \mathcal{R}_{K^*}

A paper published in 2017 did some phenomenological analysis in face of the anomalies in \mathcal{R}_K and \mathcal{R}_{K^*} , considering also leptoquarks [45]. Its content shall be briefly summed up in this section. Regarding a operator basis defined as

$$\mathcal{O}_{b_X l_Y} = (\bar{s}\gamma_\mu P_X b) (\bar{l}\gamma_\mu P_Y l) \quad \text{with } l = e, \mu \quad \text{and } X, Y = L, R \quad (2.3)$$

the ratio \mathcal{R}_K is in terms of the respective Wilson coefficients

$$\mathcal{R}_K = \frac{|C_{b_{L+R}\mu_{L-R}}|^2 + |C_{b_{L+R}\mu_{L+R}}|^2}{|C_{b_{L+R}e_{L-R}}|^2 + |C_{b_{L+R}e_{L+R}}|^2} \quad (2.4)$$

where the shorthand notation is used in which the subscript denotes what sum of coefficients is meant, e.g. $C_{b_{L+R}\mu_{L-R}} = C_{b_L\mu_L} - C_{b_L\mu_R} + C_{b_R\mu_L} - C_{b_R\mu_R}$. The formula is based on the neglect of the electromagnetic dipole operator, which is justified by the cut-off $q^2 > 1 \text{ GeV}^2$ in the observable, and "non-factorizable contributions from the weak effective Hamiltonian" [45].

For the calculation of \mathcal{R}_{K^*} one can rely on a similar formula

$$\mathcal{R}_{K^*} = \frac{(1-p) \left(|C_{b_{L+R}\mu_{L-R}}|^2 + |C_{b_{L+R}\mu_{L+R}}|^2 \right) + p \left(|C_{b_{L-R}\mu_{L-R}}|^2 + |C_{b_{L-R}\mu_{L+R}}|^2 \right)}{(1-p) \left(|C_{b_{L+R}e_{L-R}}|^2 + |C_{b_{L+R}e_{L+R}}|^2 \right) + p \left(|C_{b_{L-R}e_{L-R}}|^2 + |C_{b_{L-R}e_{L+R}}|^2 \right)} \quad (2.5)$$

in which $p \approx 0.86$ is the polarization fraction.

The most important statement was that a leptoquark representation $R_2 \sim (3, 2, 7/6)_{\text{SM}}$ could achieve a correct tuning of the branching ratio. In contrast, a particle $\tilde{R}_2 \sim (3, 2, 1/6)_{\text{SM}}$ would give the wrong correlation between \mathcal{R}_K and \mathcal{R}_{K^*} , i.e. $\mathcal{R}_K < 1 < \mathcal{R}_{K^*}$ [45, 46]. Crivellin et al. [47] pointed out that there might be unavoidable effects in the process $\mu \rightarrow e \gamma$ and transitions similar to $b \rightarrow s \mu e$, e.g. $B_s \rightarrow \mu e$. This is the basis for the investigations made later-on.

2.3. Standard Model coefficient for $\mathcal{R}_{D^{(*)}}$

Inside the SM the quark-level transition corresponding to $\mathcal{R}_{D^{(*)}}$, $b \rightarrow c \tau \bar{\nu}_\tau$ is described by the effective Hamiltonian [48]

$$\mathcal{H}_{\text{eff}} = \frac{4G_F V_{cb}}{\sqrt{2}} (\bar{c}_L \gamma_\mu b_L) (\bar{\tau}_L \gamma^\mu \nu_{\tau L}) + \text{h.c.} \quad (2.6)$$

The coefficient has a value of [49]

$$\frac{4G_F V_{cb}}{\sqrt{2}} = (1.336 \pm 0.049) \cdot 10^{-6} \text{ GeV}^{-2} . \quad (2.7)$$

3. Model basics

In this chapter, the model is presented as given by [1], first considering the fermions and the Lagrangian, then going on to the scalar sector, with basic considerations on the mass spectrum. The nomenclature is based on [50].

3.1. The new gauge group

The essence of this extended model is that the SM is only a subgroup of some larger gauge group, that has been broken down by some vacuum expectation values. The considered model is introduced via the gauge group

$$G_{\text{LQ}} = SU(4)_C \otimes SU(2)_L \otimes U(1)_R. \quad (3.1)$$

This group might again be a subgroup of $SO(10)$ or $SU(6)$ [1]. As a preliminary remark, this gauge group does not lead to proton decay as has been pointed out in general in [51] for one specific leptoquark, considered also in later chapters, and specifically for this gauge group in [52].

As with other leptoquark models the peculiarity with regard to the SM is that it unifies quarks and leptons, considering the latter as particles with the fourth color. This corresponds to the $SU(4)_C$ gauge group, where C stands for colour. The indices L and R stand for the handedness. The $SU(4)$ elements are generated by a set of matrices, which are the extension of the Gell-Mann matrices used in the $SU(3)$ group. They can be looked up in appendix A.

Broken down, the group G_{LQ} yields the known $G_{\text{SM}} = SU(3) \otimes SU(2)_L \otimes U(1)_Y$. The quantum numbers from G_{LQ} to G_{SM} are computed by

$$Y = R + \frac{\sqrt{6}}{3} T_{15} \quad , \quad (3.2)$$

where T_{15} stands for the 15th generator of the $SU(4)$ group in the basis explained in chapter A.

The electro-weak symmetry break is done by two other Higgs particles, each one acquiring a vev. Their vevs must combine together to the known $v_{\text{SM}} = 246$ GeV, so they can be parametrized using an angle β and the equations

$$v_1 = v_{\text{SM}} \cdot \sin \beta \quad \text{and} \quad v_2 = v_{\text{SM}} \cdot \cos \beta \quad , \quad (3.3)$$

resulting in $\tan \beta \in \mathbb{R}^+$ being a input parameter. On the other hand it would be unnatural to suppose quasi no mixing, i.e. $\tan \beta \rightarrow \infty$ or 0 , that's why the

3. Model basics

confinement $\tan \beta \in [1/50, 50]$ is made. The electromagnetic charge is computed by $Q = T_3^L + Y$.

Now, it is time to have a look on the fermionic representations.

3.2. Fermionic sector

3.2.1. Gauge eigenstates

The fermions in the LQ gauge are introduced as

$$F_{QL} = \begin{pmatrix} Q_L^i \\ L_L \end{pmatrix} = \begin{pmatrix} u_L^i & d_L^i \\ \nu_L & e_L \end{pmatrix} \sim (4, 2, 0)_{\text{LQ}} \sim \begin{cases} (3, 2, 1/6)_{\text{SM}} \\ (1, 2, 1/2)_{\text{SM}} \end{cases} \quad (3.4)$$

$$F_u = (\bar{u}_R^i \quad \bar{\nu}_R) \sim (\bar{4}, 1, 1/2)_{\text{LQ}} \sim \begin{cases} (\bar{3}, 1, -2/3)_{\text{SM}} \\ (1, 1, 0)_{\text{SM}} \end{cases} \quad (3.5)$$

$$F_d = (\bar{d}_R^i \quad \bar{e}_R) \sim (\bar{4}, 1, -1/2)_{\text{LQ}} \sim \begin{cases} (\bar{3}, 1, 1/3)_{\text{SM}} \\ (1, 1, -1)_{\text{SM}} \end{cases} \quad (3.6)$$

$$N \sim (1, 1, 0)_{\text{LQ}} \sim (1, 1, 0)_{\text{SM}} \quad (3.7)$$

where the index $i = 1, 2, 3$ counts the three components under the colour groups. The field N is introduced for explanation of the neutrino masses, whereas the Yukawa interactions of the particles are given as

$$-\mathcal{L}_Y \supset F_u Y_1^T H_1 F_{QL} + F_u Y_2^T \Phi F_{QL} + F_d Y_3^T H_1^\dagger F_{QL} + F_d Y_4^T \Phi^\dagger F_{QL} + F_u Y_5^T \chi N + \frac{\mu}{2} N N + \text{h.c.} \quad (3.8)$$

To obtain the small neutrino masses an inverse seesaw mechanism is chosen. For each generation, the known left-handed neutrinos ν_L are complemented by a field of right-handed neutrinos $\bar{\nu}_R$ as well as a field of Majorana neutrinos N with mass matrix μ . Its interactions and mass term are given in the last two terms in the formula above. The other terms shall be explained in chapter 3.2.2, while the procedure for the neutrino masses is given here.

The Dirac mass term between the left and right handed neutrinos is

$$M_\nu^D = \frac{v_1}{\sqrt{2}} Y_1^T - \frac{\sqrt{3}v_2}{2\sqrt{2}} Y_2^T \quad (3.9)$$

and between the right-handed and the Majorana neutrinos

$$M_\chi^D = \frac{v_\chi}{\sqrt{2}} Y_5^T. \quad (3.10)$$

Hence, the resulting mass matrix for the neutrinos is:

$$(\nu_L \quad \bar{\nu}_R \quad N) \begin{pmatrix} 0 & M_\nu^D & 0 \\ M_\nu^{D,T} & 0 & M_\chi^D \\ 0 & M_\chi^{D,T} & \mu \end{pmatrix} \begin{pmatrix} \nu_L \\ \bar{\nu}_R \\ N \end{pmatrix} \quad (3.11)$$

This matrix possesses now three light eigenstates without the necessity of any fine-tuning.

Having set up all fermions and their interactions, it is now time to parametrize the particles' masses and the present variables in a convenient fashion.

3.2.2. The fermions' masses

For the sake of simplicity, in this subsection the mass eigenstates are denoted with a tilde, this sign is omitted again in subsequent sections.

Regarding the charged leptons, the basis is chosen such that their mass matrix is diagonal, i.e. they don't mix in this basis. But in the quark sector, it is possible to assume mixing within every subset of quark type:

$$\begin{aligned} u_L &= V_u \tilde{u}_L \\ u_R &= U_u \tilde{u}_R \Rightarrow \bar{u}_R = \bar{\tilde{u}}_R U_u^\dagger \\ d_L &= V_d \tilde{d}_L \\ d_R &= U_d \tilde{d}_R \Rightarrow \bar{d}_R = \bar{\tilde{d}}_R U_d^\dagger \end{aligned} \quad (3.12)$$

These mixings give together with the interaction written in eq. 3.8 the mass terms

$$\begin{aligned} U_u^\dagger \hat{M}_u V_u &= \frac{v_1}{\sqrt{2}} Y_1^T + \frac{v_2}{2\sqrt{6}} Y_2^T \\ U_d^\dagger \hat{M}_d V_d &= \frac{v_1}{\sqrt{2}} Y_3^T + \frac{v_2}{2\sqrt{6}} Y_4^T \\ \hat{M}_e &= \frac{v_1}{\sqrt{2}} Y_3^T - \frac{3v_2}{2\sqrt{6}} Y_4^T \end{aligned} \quad (3.13)$$

The particles' masses are known (see e.g. [49]) and expressed in the formula with the diagonal $\hat{M}_p \equiv \hat{Y}_p v_{\text{SM}}/\sqrt{2}$ matrices for particle p . To arrive at Yukawa couplings in accordance with the fermion masses, one rearranges the above equations to

$$\begin{aligned} Y_1^T &= \frac{\sqrt{1 + \tan^2 \beta}}{\tan \beta} V_u^\dagger \hat{Y}_u U_u + \frac{\sqrt{3}}{6 \tan \beta} Y_2^T \\ Y_3^T &= \frac{1}{4} \frac{\sqrt{1 + \tan^2 \beta}}{\tan \beta} \left(3V_d^\dagger \hat{Y}_d U_d + \hat{Y}_e \right) \\ Y_4^T &= \frac{\sqrt{3}}{2} \sqrt{1 + \tan^2 \beta} \left(V_d^\dagger \hat{Y}_d U_d - \hat{Y}_e \right) \end{aligned} \quad (3.14)$$

3. Model basics

Here Y_2 has already been chosen to be a input parameter: in eq. 3.11, there are three matrices and one has to be used to set the light neutrino masses, which now is μ . So the other two Yukawa couplings Y_2 and Y_5 are free input.

It is noteworthy that in the limit $\tan \beta \gg 1$ both Y_1 and Y_3 converge to constant values, while $Y_4 \propto \tan \beta$. For the complementary limit $\tan \beta \ll 1$, Y_4 becomes a constant and the other two get enhanced, with $Y_1, Y_3 \propto 1/\tan \beta$.

Another constraint on the couplings is the demand that they should be symmetric: $Y_i^T = Y_i$. This is done firstly to limit the parameter space. But secondly, it would be a natural consequence when breaking down to G_{LQ} from a greater gauge group, for example $SO(10)$. As one can easily reproduce, the symmetry of the Yukawa matrices implies the relation between the mixing matrices

$$U_d = V_d^* \quad \text{and} \quad U_u = V_u^* . \quad (3.15)$$

Going on, the so-called Cabibbo-Kobayashi-Maskawa (CKM) matrix is defined as the product of the left-handed quark's mixing:

$$V_{\text{CKM}} = V_u^\dagger V_d \quad (3.16)$$

This matrix is known and thus constrains again the parameter space that can be chosen for the mixing. Both upper formulae leave now only one mixing matrix free to choose, parametrized by three angles θ_{kl} and a phase δ . This matrix has been chosen to be

$$V_d = \begin{pmatrix} c_{12}c_{13} & s_{12}c_{13} & s_{13}e^{-i\delta} \\ -s_{12}c_{23} - c_{12}s_{23}s_{13}e^{i\delta} & c_{12}c_{23} - s_{12}s_{23}s_{13}e^{i\delta} & s_{23}c_{13} \\ s_{12}s_{23} - c_{12}c_{23}s_{13}e^{i\delta} & -c_{12}s_{23} - s_{12}c_{23}s_{13}e^{i\delta} & c_{23}c_{13} \end{pmatrix} \quad (3.17)$$

where $s_{kl} = \sin \theta_{kl}$ and $c_{kl} = \cos \theta_{kl}$.

Regarding the neutrinos, a 9×9 matrix describes the mixing, defined in analogy to before, it is

$$\begin{pmatrix} \nu_L \\ \nu_R \\ N \end{pmatrix} = U_\nu \begin{pmatrix} \nu_1 \\ \vdots \\ \nu_9 \end{pmatrix} . \quad (3.18)$$

Just like in the quark sector, the mixing between the SM neutrinos is a measured quantity, known as the Pontecorvo–Maki–Nakagawa–Sakata (PMNS) matrix. Assuming the known neutrinos to be in the first three components one arrives at the constraint

$$V_{\text{PMNS},mn} \simeq U_{\nu,mn} \quad \text{with} \quad m, n = 1, 2, 3 \quad (3.19)$$

for the submatrix of the neutrino mixing. Note that the 3×3 submatrix of U_ν can not be unitary in contrast to the PMNS matrix. The deviation from unitarity lies within the current errors of the measurements of the PMNS matrix, though.

The proof was done through a rough calculation by Rösch [53]. In order to project out the different interaction states, the following submatrices are defined:

$$U_\nu = \begin{pmatrix} U_{\nu,L} \\ U_{\nu,R} \\ U_{\nu,N} \end{pmatrix} \quad (3.20)$$

Each of these matrices $U_{\nu,\{L,R,N\}}$ is a 3×9 matrix.

3.3. Scalar sector

3.3.1. Scalars' spectrum

The $SU(4)$ breaking particle is modelled by

$$\chi = \begin{pmatrix} \bar{S}_1^{\dagger,i} \\ \chi^0 \end{pmatrix}, \quad i = 1, 2, 3 \quad (3.21)$$

and it transforms under G_{LQ} as $\chi \sim (4, 1, 1/2)_{LQ}$ and in the SM gauge as $\bar{S}_1^{\dagger} \sim (3, 1, 2/3)_{SM}$ and $\chi^0 \sim (1, 1, 0)_{SM}$. The field yields a vacuum expectation value in the last component, which breaks the $SU(4)$ group, parametrized by

$$\langle \chi^0 \rangle = \frac{v_\chi}{\sqrt{2}} \quad (3.22)$$

The vev controls the mass of the vector leptoquark U_1 (see the subsequent section 3.4) with $m_{U_1} = g_s \cdot v_\chi / 2$, where g_s is the strong coupling. Because this particle would give significant contributions to K meson decays, the constraint of the $K_L^0 \rightarrow e^\pm \mu^\mp$ process limits the mass of the vector leptoquark to $m_{U_1} \geq 1.6 \cdot 10^3$ TeV, thus a value $v_\chi \geq 4 \cdot 10^6$ GeV [54].

Another scalar particle is furthermore introduced with a Higgs doublet

$$H_1 = \begin{pmatrix} H_1^+ \\ H_1^0 \end{pmatrix} \sim (1, 2, 1/2)_{LQ,SM}, \quad \text{where } \langle H_1^0 \rangle = \frac{v_1}{\sqrt{2}} \quad (3.23)$$

The leptoquarks come into place by considering a representation that transforms as $(15, 2, 1/2)_{LQ}$, which can be displayed as

$$\Phi = \begin{pmatrix} G^{ij} & R_2^j \\ \tilde{R}_2^i & 0 \end{pmatrix} + T_{15} H_2, \quad i, j = 1, 2, 3 \quad (3.24)$$

Each of these particle has still two components in the $SU(2)$ space. Note that there is an additional Higgs doublet H_2 included inside of this scalar. The components have the following SM quantum numbers:

- $G \sim (8, 2, 1/2)_{SM}$, being a scalar gluon, mediates quark-quark interactions
- $\tilde{R}_2 \sim (\bar{3}, 2, -1/6)_{SM}$ is the first scalar leptoquark

3. Model basics

- $R_2 \sim (3, 2, 7/6)_{\text{SM}}$ is the second scalar leptoquark
- $H_2 \sim (1, 2, 1/2)_{\text{SM}}$ has the same quantum numbers as the H_1 , acquiring the vev $\langle H_2^0 \rangle = \frac{v_2}{\sqrt{2}}$

An overview of all the scalar particles is given in tab. 3.1.

G_{LQ}	G_{SM}	G_{31}
$\Phi \sim (15, 2, 1/2)$	$R_2 \sim (3, 2, 7/6)$	$R_2^{5/3} \sim (3, 5/3)$ $R_2^{2/3} \sim (3, 2/3)$
	$\tilde{R}_2^\dagger \sim (\bar{3}, 2, -1/6)$	$\tilde{R}_2^{\dagger, 1/3} \sim (\bar{3}, 1/3)$ $\tilde{R}_2^{\dagger, -2/3} \sim (\bar{3}, -2/3)$
	$G \sim (8, 2, 1/2)$	$G^+ \sim (8, 1)$ $G^0 \sim (8, 0)$
	$H_2 \sim (1, 2, 1/2)$	$H_2^+ \sim (1, 1)$ $H_2^0 \sim (1, 0)$
$\chi \sim (4, 1, 1/2)$	$\tilde{S}_1^\dagger \sim (3, 1, 2/3)$	$\sim (3, 2/3)$
	$\chi^0 \sim (1, 1, 0)$	$\sim (1, 0)$
$H_1 \sim (1, 2, 1/2)$	$\sim (1, 2, 1/2)$	$H_1^+ \sim (1, 1)$ $H_1^0 \sim (1, 0)$

Table 3.1.: Compact view of the different components of the new scalar particle spectrum.

3.3.2. Scalar potential

The potential of the scalar particles is expressed by

$$\begin{aligned}
-\mathcal{L} \supset & m_H^2 H_1^\dagger H_1 + m_\chi^2 \chi^\dagger \chi + m_\Phi^2 \text{Tr}(\Phi^\dagger \Phi) + \lambda_1 H_1^\dagger H_1 \chi^\dagger \chi + \\
& + \lambda_2 H_1^\dagger H_1 \text{Tr}(\Phi^\dagger \Phi) + \lambda_3 \chi^\dagger \chi \text{Tr}(\Phi^\dagger \Phi) + \left(\lambda_4 H_1^\dagger \chi^\dagger \Phi \chi + \text{h.c.} \right) + \\
& + \lambda_5 H_1^\dagger \text{Tr}(\Phi^\dagger \Phi) H_1 + \lambda_6 \chi^\dagger \Phi^\dagger \Phi \chi + \lambda_7 \left(H_1^\dagger H_1 \right)^2 + \\
& + \lambda_8 \left(\chi^\dagger \chi \right)^2 + \lambda_9 \text{Tr} \left(\left(\Phi^\dagger \Phi \right)^2 \right) + \lambda_{10} \left(\text{Tr}(\Phi^\dagger \Phi) \right)^2
\end{aligned} \tag{3.25}$$

where the traces are taken only within the $SU(4)$ space. The parameters m_H^2 , m_χ^2 and m_Φ^2 are eliminated using the tadpole equations. For now, the ten couplings are left as free to choose. Some of them, however, will be discussed in section 3.3.4.

This potential, however, is not the most general one, but is missing some combinations of the scalar fields. As will be discussed in section 3.3.4, this leads to quasi-degenerate masses for some of the scalars. In the most general form, one

would have more parameters and thus more degrees of freedom when setting the scalars' masses.

3.3.3. Mixing

Turning to the scalar mixing, one should have a closer look to tab. 3.1. When looking at the electromagnetic charge Q , it is noticeable that both scalar leptoquarks mix in their second $SU(2)$ -component together with the \bar{S}_1^\dagger .

While the first components of the scalar leptoquarks don't mix with any other particle, the mixing of the mentioned three particles is defined as

$$\begin{pmatrix} R_2^{2/3} \\ \tilde{R}_2^{2/3} \\ \bar{S}_1^\dagger \end{pmatrix} = Z^{\text{LQ}} \begin{pmatrix} G_{U_1} \\ R'_{(2)} \\ R'_{(3)} \end{pmatrix}. \quad (3.26)$$

As hinted in the equation, one state is the Goldstone boson for the vector leptoquark U_1 . A convention is now introduced to shorten the specification of the particles:

$$\begin{aligned} \tilde{R}_2^{1/3} &\rightarrow \tilde{R}_2 \\ R_2^{5/3} &\rightarrow R_2 \end{aligned} \quad (3.27)$$

The next particles to look at are the Higgs fields. The fields can be parametrized as usual by

$$H_{1,2} = \begin{pmatrix} H_{1,2}^+ \\ v_{1,2} + \phi_{1,2} + iA_{1,2} \end{pmatrix} \quad (3.28)$$

and in a similar fashion the χ^0 field. Then, the components mix as

$$\begin{pmatrix} H_1^+ \\ H_2^+ \end{pmatrix} = Z^{h^+} \begin{pmatrix} G_W \\ h^+ \end{pmatrix} \quad (3.29)$$

$$\begin{pmatrix} \phi_1 \\ \phi_\chi \\ \phi_2 \end{pmatrix} = Z^h \begin{pmatrix} h_1 \\ h_2 \\ h_3 \end{pmatrix} \quad (3.30)$$

$$\begin{pmatrix} A_1 \\ A_\chi \\ A_2 \end{pmatrix} = Z^A \begin{pmatrix} G_Z \\ G_{Z'} \\ A \end{pmatrix} \quad (3.31)$$

where one of the charged Higgs becomes the Goldstone of the W boson, and pseudo scalar fields give mass to Z and Z' , see 3.4.

The scalar gluon can be decomposed into three particles, one charged G^+ and two uncharged $G_{(1,2)}^0$, analogous to eq. 3.28. Their masses, however, will be degenerate due to the incomplete scalar potential.

3.3.4. Transformation into mass eigenstates

Regarding the masses, the actual steps were done automatically by SARAH [36–39]. One arrives at the mass matrices and their eigenvalues that are presented in this section. As a convention the mass matrices are denoted by a capital M and the eigenvalues are called m .

In the model, there are ten scalars' masses to be calculated. Now, apart from $\tan\beta$ and the vev v_χ , the masses are determined by the ten couplings λ_i in eq. 3.25.

Looking at the matrices, one sees that the mass of the pseudo-scalar depends on only one coupling, with the corresponding mass matrix being

$$M_A^2 = \begin{pmatrix} \frac{1}{4}\sqrt{3}\lambda_4 \cot(\beta)v_\chi^2 & 0 & -\frac{1}{4}\sqrt{3}\lambda_4 v_\chi^2 \\ 0 & 0 & 0 \\ -\frac{1}{4}\sqrt{3}\lambda_4 v_\chi^2 & 0 & \frac{1}{4}\sqrt{3}\lambda_4 \tan(\beta)v_\chi^2 \end{pmatrix}. \quad (3.32)$$

The non-zero eigenvalue follows the equation

$$m_A^2 = \frac{\sqrt{3}}{4}\lambda_4 (\tan^2(\beta) + 1) \cot(\beta)v_\chi^2 = \frac{\sqrt{3}}{2}\lambda_4 \sin(2\beta)v_\chi^2 \quad (3.33)$$

By specifying a mass for the pseudo-scalar, one can substitute λ_4 in the equation for the mass of h^+ , which is described by the matrix

$$M_{h^+}^2 = \begin{pmatrix} -\frac{\lambda_5 \tan^2(\beta)v_{\text{SM}}^2}{2(\tan^2(\beta)+1)} - \frac{\sqrt{3}}{4}\tan(\beta)\lambda_4 v_\chi^2 & \frac{1}{4}\left(\frac{2\lambda_5 \tan(\beta)v_{\text{SM}}^2}{\tan^2(\beta)+1} - \sqrt{3}\lambda_4 v_\chi^2\right) \\ \frac{1}{4}\left(\frac{2\lambda_5 \tan(\beta)v_{\text{SM}}^2}{\tan^2(\beta)+1} - \sqrt{3}\lambda_4 v_\chi^2\right) & -\frac{2\lambda_5 \tan(\beta)v_{\text{SM}}^2 - \sqrt{3}\lambda_4 (\tan^2(\beta)+1)v_\chi^2}{4(\tan^3(\beta)+\tan(\beta))} \end{pmatrix} \quad (3.34)$$

This leaves the formula with a dependence only on λ_5 , which is determined by the mass through

$$m_{h^+}^2 = \frac{1}{4}\cot(\beta)\left(\sqrt{3}\lambda_4 (\tan^2(\beta) + 1) v_\chi^2 - 2\lambda_5 \tan(\beta)v_{\text{SM}}^2\right) \quad (3.35)$$

$$= m_A^2 - \frac{1}{2}\lambda_5 \tan(\beta)v_{\text{SM}}^2 \quad (3.36)$$

Note that the value of λ_5 specifies the mass difference between the charged Higgs h^+ and the pseudo-scalar A , but only suppressed by v_{SM}/v_χ .

For the following calculations, two parameters are introduced to simplify expressions, by

$$\eta := \frac{\lambda_9}{\tan^2(\beta) + 1} v_{\text{SM}}^2 \quad (3.37)$$

$$\alpha := \frac{1}{8}\lambda_6 v_\chi^2 \quad (3.38)$$

So, unless λ_6 , λ_9 , and $\tan\beta$ are tuned, α is a non-negligible contribution to the masses, whereas η is only a suppressed term. Looking at the mass equation for the two scalar leptoquarks R_2 and \tilde{R}_2 ,

$$m_{R_2}^2 = \frac{v_\chi^2}{8} \left(2\sqrt{3}\lambda_4 \tan(\beta) - 3\lambda_6 \right) + \frac{v_{\text{SM}}^2 (\lambda_9 - 3\lambda_5 \tan^2(\beta))}{6 (\tan^2(\beta) + 1)} \quad (3.39)$$

$$= \frac{\tan^2(\beta)}{\tan^2(\beta) + 1} m_{h^+}^2 - 3\alpha + \frac{\eta}{6} \quad (3.40)$$

$$m_{\tilde{R}_2}^2 = \frac{v_\chi^2}{8} \left(2\sqrt{3}\lambda_4 \tan(\beta) + \lambda_6 \right) - \frac{v_{\text{SM}}^2 (\lambda_5 \tan^2(\beta) + \lambda_9)}{2 (\tan^2(\beta) + 1)} \quad (3.41)$$

$$= \frac{\tan^2(\beta)}{\tan^2(\beta) + 1} m_{h^+}^2 + \alpha - \frac{\eta}{2} \quad (3.42)$$

$$m_{\tilde{R}_2}^2 - m_{R_2}^2 = \frac{\lambda_6 v_\chi^2}{2} - \frac{2\lambda_9}{3 (\tan^2(\beta) + 1)} v_{\text{SM}}^2 = 4\alpha - \frac{2\eta}{3} \quad (3.43)$$

one can see that through the previous calculations these masses depend only on α and η or λ_6 and λ_9 , respectively. Furthermore, it's visible that λ_6 controls which of the two particles is lighter and is fixed through setting one of the leptoquark masses. The correction by λ_9 is negligible here due to its suppression with v_{SM}^2/v_χ^2 .

Three of the remaining masses are now – up to λ_9 correction – determined: the mass of the scalar colour-octet G

$$m_G^2 = m_{R_2}^2 - \frac{2}{3}\eta \quad (3.44)$$

and – after projecting out the matrix' zero eigenvalue – and the masses of R'

$$M_{R'}^2 = \begin{pmatrix} -\frac{1}{8}v_\chi^2 (\lambda_6 - 2\sqrt{3}\lambda_4 \tan(\beta)) + \frac{\eta}{2} & -\frac{1}{4}v_\chi^2 \lambda_6 \kappa \\ -\frac{1}{4}v_\chi^2 \lambda_6 \kappa & -\frac{v_\chi^2}{8} (\lambda_6 - 2\sqrt{3}\lambda_4 \tan(\beta)) \kappa^2 \end{pmatrix} \quad (3.45)$$

with $\kappa = \sqrt{1 + \frac{8v_{\text{SM}}^2}{3v_\chi^2 (\tan^2(\beta) + 1)}} \approx 1$. When setting $\kappa = 1$ as an approximation, but still minding η , the corresponding eigenvalues are

$$m_{R'_{(2)}}^2 = \frac{1}{4} \left(\sqrt{3}\lambda_4 \tan(\beta) v_\chi^2 - 4\alpha - \sqrt{64\alpha^2 + \eta^2} + \eta \right) \quad (3.46)$$

$$\approx \frac{1}{4} \sqrt{3}\lambda_4 \tan(\beta) v_\chi^2 - 3\alpha + \frac{\eta}{4} - \frac{\eta^2}{64\alpha} \quad (3.47)$$

$$m_{R'_{(3)}}^2 = \frac{1}{4} \left(\sqrt{3}\lambda_4 \tan(\beta) v_\chi^2 - 4\alpha + \sqrt{64\alpha^2 + \eta^2} + \eta \right) \quad (3.48)$$

$$\approx \frac{1}{4} \sqrt{3}\lambda_4 \tan(\beta) v_\chi^2 + \alpha + \frac{\eta}{4} + \frac{\eta^2}{64\alpha} \quad (3.49)$$

In the limit $\tan \beta \gg 1$ the term proportional to λ_4 is approximately m_A^2 . If m_A is chosen to be higher than the SM contributions, the latter can be neglected and one yields $m_{R'_{(1)}} = m_{R_2}$ and $m_{R'_{(2)}} = m_{\tilde{R}_2}$, deviating only up to few percent.

3. Model basics

The same counts for the scalar gluon, as η gets smaller for large values of $\tan\beta$ and it follows $m_G = m_{R_2}$. This degeneration is however a mere consequence of the incomplete potential. Adding the missing combinations to arrive at the most general form, one would yield also couplings that result in a non-negligible mass difference between the scalar gluon G and the scalar leptoquark R_2 .

Note that for $\tan\beta \leq 1$ all the scalar leptoquarks naively become light as the first terms in each eq. 3.40, 3.43, 3.47 and 3.49 will be small.

To conclude, it is possible to divide these particles in two set: On the one hand, there is the mass of R_2 , which determines – up to some corrections – the mass of $R'_{(1)}$ and the mass of the colour octet G , too. On the other hand, there is the mass of the pseudo-scalar A , approximately equal to the mass of charged Higgs h^+ and the masses of the other two scalar leptoquarks which, depending on $\tan\beta$ and α , are higher than m_A .

Thus, two input parameter can be chosen to set up the masses of these particles: the high masses' scale with m_A and the lower masses by choosing m_{R_2} .

3.3.5. Fixing the neutral Higgs mass

These considerations have left only the uncharged Higgs particles untouched. The corresponding mass matrix is under-determined with respect to the couplings and one of the diagonal entries is already close to an eigenvalue:

$$\begin{aligned}
M_h^2 = & v_\chi^2 \begin{pmatrix} -\frac{\sqrt{3}\lambda_4(\tan(\beta)^2+1)}{4(\tan(\beta)^3+\tan(\beta))} & 0 & \frac{\sqrt{3}\lambda_4}{4} \\ 0 & 2\lambda_8 & 0 \\ \frac{\sqrt{3}\lambda_4}{4} & 0 & -\frac{1}{4}\sqrt{3}\lambda_4 \tan(\beta) \end{pmatrix} + \\
& + v_\chi v_{\text{SM}} \begin{pmatrix} 0 & \frac{\sqrt{3}\lambda_4+2\lambda_1 \tan(\beta)}{2\sqrt{\tan(\beta)^2+1}} & 0 \\ \frac{\sqrt{3}\lambda_4+2\lambda_1 \tan(\beta)}{2\sqrt{\tan(\beta)^2+1}} & 0 & \frac{4\lambda_3+3\lambda_6+2\sqrt{3}\lambda_4 \tan(\beta)}{4\sqrt{\tan(\beta)^2+1}} \\ 0 & \frac{4\lambda_3+3\lambda_6+2\sqrt{3}\lambda_4 \tan(\beta)}{4\sqrt{\tan(\beta)^2+1}} & 0 \end{pmatrix} + \\
& + v_{\text{SM}}^2 \begin{pmatrix} \frac{2\lambda_7 \tan(\beta)^3}{\tan(\beta)^3+\tan(\beta)} & 0 & \frac{\lambda_2 \tan(\beta)}{\tan(\beta)^2+1} \\ 0 & 0 & 0 \\ \frac{\lambda_2 \tan(\beta)}{\tan(\beta)^2+1} & 0 & \frac{12\lambda_{10}+7\lambda_9}{6(\tan(\beta)^2+1)} \end{pmatrix}
\end{aligned} \tag{3.50}$$

where $m_{h_3} \approx 2\lambda_8 v_\chi^2$. In an approximation with $v_{\text{SM}} = 0$, the matrix has the eigenvalues $\left\{0, \frac{1}{4}\sqrt{3}\lambda_4 \frac{\tan^2(\beta)+1}{\tan(\beta)} v_{\text{PS}}^2, 2\lambda_8 v_{\text{PS}}^2\right\}$, where the second entry is equal to m_A^2 .

This motivates the application of a seesaw-approximation to first order, to simplify the lengthy calculations and fix the lightest eigenvalue at 125 GeV. Therefore λ_8 can be set equal to 0.2, which is motivated firstly to justify the approximation

that necessitates the condition $\lambda_4 \ll \lambda_8$. But also secondly, in order to get the corresponding Higgs mass near the scale of symmetry breaking v_χ .

The matrix depends on the free parameters $\lambda_1, \lambda_2, \lambda_3, \lambda_7, \lambda_8, \lambda_9$, and λ_{10} . Applying the approximation, one arrives at the matrix

$$\begin{aligned}
 M_h^2 &\approx M_{h,SSA}^2 - \delta M_{h,SSA}^2 \\
 &= \begin{pmatrix} \frac{\sqrt{3}\lambda_4}{4(\tan^2(\beta)+1)} & -\frac{1}{4}\sqrt{3}\lambda_4 \\ -\frac{1}{4}\sqrt{3}\lambda_4 & \frac{1}{4}\sqrt{3}\lambda_4 \tan(\beta) \end{pmatrix} v_\chi^2 + \begin{pmatrix} \frac{8\lambda_7 \tan^2(\beta)}{4} & \lambda_2 \tan(\beta) \\ \lambda_2 \tan(\beta) & \frac{12\lambda_{10}+7\lambda_9}{6} \end{pmatrix} \frac{v_{SM}^2}{\tan^2(\beta)+1} - \\
 &\quad - \begin{pmatrix} (\sqrt{3}\lambda_4 - 2\lambda_1 \tan(\beta))^2 & (2\lambda_1 \tan(\beta) - \sqrt{3}\lambda_4) \gamma \\ (2\lambda_1 \tan(\beta) - \sqrt{3}\lambda_4) \gamma & \gamma^2 \end{pmatrix} \cdot \frac{v_{SM}^2}{8\lambda_8 (\tan^2(\beta)+1)}, \tag{3.51}
 \end{aligned}$$

where $\gamma = \frac{3}{2}\lambda_6 + 2\lambda_3 - 1\sqrt{3}\lambda_4 \tan(\beta)$ was used for reasons of shortness and $M_{h,SSA}^2$ was split into two terms, proportional to v_{SM}^2 and v_χ^2 , respectively.

λ_7 is the coupling for the quartic H_1 coupling, which makes it primarily suitable for setting the correct SM Higgs mass to the known 125 GeV, especially in the limit $\tan \beta \gg 1$. In that limit the vevs follow $v_1 = v_{SM}$ and $v_2 \rightarrow 0$, so h_1 can indeed be regarded as the SM Higgs particle, and furthermore this limit is needed for the purpose of explaining the anomalies, see chapter 5.5. Also, together with λ_{10} , it appears only once in the expression, which makes it easier to rearrange it into a solution. Solving the equation and implementing the resulting function in the SPheno input files, the h_1 mass is fixed up to machine precision.

3.4. Gauge bosons

Regarding the gauge bosons, the SM set is extended and additionally described by the multiplet

$$A_\mu = \begin{pmatrix} G_\mu & U_{1,\mu}/\sqrt{2} \\ U_{1,\mu}^*/\sqrt{2} & 0 \end{pmatrix} + T_{15} B'_\mu \sim (15, 1, 0)_{LQ} \tag{3.52}$$

The field $G_\mu \sim (8, 1, 0)_{SM}$ are the SM gluons and $U_{1,\mu} \sim (3, 1, 2/3)_{SM}$ is the vector leptoquark, while B'_μ mixes together with the B_μ gauge field of the $U(1)_R$ group and the $SU(2)_L$ gauge field W_μ to the known W and Z bosons plus an additional Z' , as well as the photon. The mass of both, the vector leptoquark and Z' lie at the scale of $SU(4)$ breaking. The gauge bosons are not further relevant for the phenomenological examinations in this work.

4. Phenomenological considerations

In this chapter the relevant new Feynman graphs are presented and remarks are made on the mixing matrix Z^{LQ} . Last but not least the Wilson coefficients due to the new particles for the anomalies are calculated at tree-level as well as the additional loop diagram by G^- in $b \rightarrow s\gamma$.

4.1. New graphs

Here, some basic graphs shall be presented that contribute to the processes and which are expected to be of relevant magnitudes.

$\mathcal{R}_{K^{(*)}}$

The decay underlying $\mathcal{R}_{K^{(*)}}$ receives a tree-level contribution through the down-quark-lepton-coupling of R' , see 4.1. This means that it is not suppressed by the mixing because the same interaction state is concerned with both vertices.

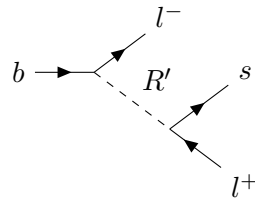


Figure 4.1.: Tree-level graph via the scalar leptoquark R' to the process $b \rightarrow s l l$.

$\mathcal{R}_{D^{(*)}}$

Here, the R' adds a tree-level graph to the decay, as well, see 4.2. But, except for one term, the two different interaction states that are mixed within R' enter in this decay: one on the $u-\nu$ -, the other on the $d-l$ -vertex.

$B \rightarrow X_s \gamma$

In this process, the new scalar gluon can mediate through each of its representations, and either an up-type or a down-type quark, for the charged and the uncharged scalar gluon(s), see 4.3.

4. Phenomenological considerations

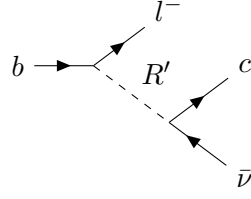


Figure 4.2.: Tree-level graph via the scalar leptoquark R' to the process $b \rightarrow c l \bar{\nu}$.



Figure 4.3.: New loop contributions via the scalar gluons, with either up- or down-type quarks, contributing to $b \rightarrow s \gamma$.

Lepton Flavour Violating decays

As mentioned, the LFV decay $\mu \rightarrow e \gamma$ gives crucial constraints when trying to explain the anomaly in $\mathcal{R}_{K^{(*)}}$. It corresponds to the same vertices as the $b \rightarrow s l^+ l^-$ process. As the photon can induce effects through penguin-type diagrams, constraints from $\mu^- \rightarrow e^- e^+ e^-$ might get violated as well. Additionally, the latter process receives contributions through box-type diagrams via leptoquark-quark loops as in fig. 4.6.

Similarly, the muonic decays can be mediated through R_2 - u loops, as well, but also the extended neutrino sector does contribute to the processes, either with the SM W -boson or the charged Higgs h^+ . The diagrams are depicted in fig. 4.4 and 4.5, respectively.

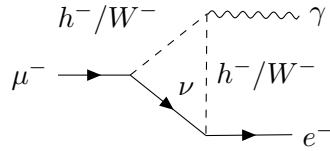


Figure 4.4.: Possible dominant contribution to the $\mu \rightarrow e \gamma$ process if the six additional neutrinos are light enough.

Leptonic meson decays

Just as to $\mathcal{R}_{K^{(*)}}$, the leptoquark contributes via tree-level to the leptonic decay of a meson consisting of two down-type quarks, see fig. 4.7. Examples for these decays are the processes $K_L^0 \rightarrow e^\pm \mu^\mp$ and $B_s \rightarrow \mu^+ \mu^-$.

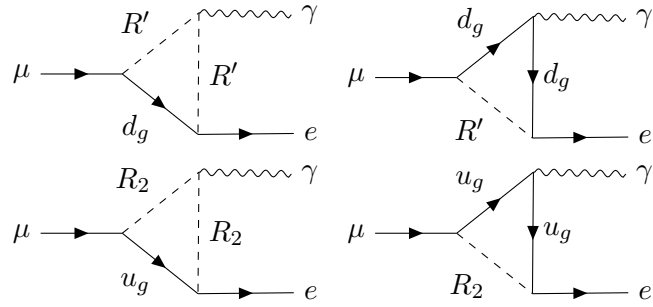


Figure 4.5.: Contributions from the leptoquarks R' (upper diagrams) and R_2 (lower diagrams) to the decay $\mu \rightarrow e \gamma$.

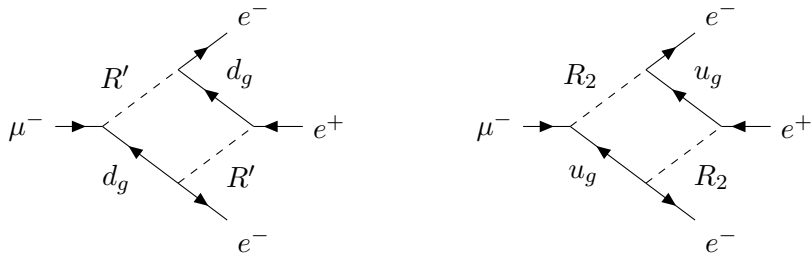


Figure 4.6.: Box diagram via leptoquark-quark loops to the process $\mu^- \rightarrow e^- e^+ e^-$.

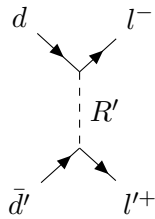


Figure 4.7.: Tree-level graph via the scalar leptoquark R' to the process $M \rightarrow l^- l^+$, where M consists of two down-type quarks.

4.2. The mixing matrix of the scalar leptoquarks

Because the mixing of the R' plays a crucial role especially in the Wilson coefficient of $\mathcal{R}_{D^{(*)}}$, it shall be discussed in this separate chapter. As shall be proven here, the matrix does not provide any mixing large enough for the purposes of explaining $\mathcal{R}_{D^{(*)}}$, unless at some fine-tuned points in parameter space that are not of interest. This will allow for restricting the discussion of the present Wilson coefficients to only one term.

As mentioned before the mixing matrix Z^{LQ} is the rotation between the three interaction states \bar{S}_1^\dagger , $R_2^{2/3}$ and $\tilde{R}_2^{2/3}$, yielding the Goldstone boson for the vector leptoquark and two massive states. The mixing matrix is given by

$$\begin{aligned}
 Z_{(3)}^{\text{LQ}} = & \begin{pmatrix} 0 & 1 & 0 \\ 0 & 0 & 1 \\ 1 & 0 & 0 \end{pmatrix} + \frac{2v_{\text{SM}}}{\sqrt{3}\sqrt{\tan^2(\beta)+1}v_{\text{PS}}} \begin{pmatrix} -1 & 0 & 0 \\ -1 & 0 & 0 \\ 0 & 1 & 1 \end{pmatrix} - \\
 & - \frac{v_{\text{SM}}^2}{3(\tan^2(\beta)+1)v_{\text{PS}}^2} \begin{pmatrix} 0 & 2 & \frac{3\lambda_9-4\sqrt{3}\lambda_4\tan(\beta)+6\lambda_6}{2\lambda_6} \\ 0 & \frac{4\sqrt{3}\lambda_4\tan(\beta)+2\lambda_6-3\lambda_9}{2\lambda_6} & 2 \\ 4 & 0 & 0 \end{pmatrix} + \\
 & + \frac{v_{\text{SM}}^3}{3\sqrt{3}(\tan^2(\beta)+1)^{3/2}v_{\text{PS}}^3} \cdot \\
 & \cdot \begin{pmatrix} 8 & 0 & 0 \\ 8 & 0 & 0 \\ 0 & \frac{3\lambda_9-4\sqrt{3}\lambda_4\tan(\beta)-6\lambda_6}{\lambda_6} & \frac{-10\lambda_6-3\lambda_9+4\sqrt{3}\lambda_4\tan(\beta)}{\lambda_6} \end{pmatrix}
 \end{aligned} \tag{4.1}$$

where a series expansion has already been done around $v_{\text{SM}} = 0$ up to third order in order to obtain a more compact and readable expression. The approximation is justified up to high precision deduced from the fact that both vevs are basically fixed. One can substitute $v_{\text{SM}}/v_\chi \rightarrow x$ and rearrange the components in powers of x . As discussed in section 3.3, it is $x \approx 6 \cdot 10^{-5}$. The matrix shall be discussed up to second order now. It is obvious that the third order term is suppressed too much to give terms $O(0.1)$ in Z^{LQ} .

It also is clear that the first order terms can't change the mixing as they are equal to $2x/\sqrt{3}$ or suppressed, for low or high values of $\tan\beta$, respectively.

The coefficient for x^2 in the elements (2,2) or (1,3) can be rearranged in terms of the masses which are chosen to be input parameters. Starting with the complete expression

$$\frac{1}{3(\tan^2\beta+1)} - \frac{\lambda_9}{2\lambda_6(\tan^2\beta+1)} + \frac{2\sqrt{3}\tan\beta\lambda_4}{3\lambda_6(\tan^2\beta+1)} \stackrel{!}{=} O(10^8) \tag{4.2}$$

one of these three terms should be at the order of magnitude of 10^8 in order to

counterbalance the suppression by $x^2 = 3.8 \cdot 10^{-9}$.

This is not possible for the first term, the second however can fulfil the requirement with

$$\begin{aligned}
 \tan \beta &\approx 0.1 \\
 \lambda_9 &\approx -1 \\
 \lambda_6 &\approx 7.2 \cdot 10^{-8} \\
 \Rightarrow \alpha &\approx 1.44 \cdot 10^5 \text{ GeV}^2 .
 \end{aligned} \tag{4.3}$$

This implies for the mass of \tilde{R}_2 :

$$\begin{aligned}
 m_{\tilde{R}_2} &= \sqrt{m_{R_2}^2 + 5.76 \cdot 10^5 \text{ GeV}^2} \in [930, 1693] \text{ GeV} \\
 \Rightarrow m_{\tilde{R}_2} - m_{R_2} &= [193, 430] \text{ GeV}
 \end{aligned} \tag{4.4}$$

having inserted typical values $m_{R_2} \in [0.5, 1.5] \text{ TeV}$, see the later chapter 5.5.

With these values, one can arrive at a mixing of few percent, for this point there was still no effect in $\mathcal{R}_{D^{(*)}}$, though. Even more, $\mathcal{R}_{K^{(*)}}$ couldn't be tuned due to the choice of $\tan \beta$ (see section 5.5) and due to the fact that \tilde{R}_2 favours $\mathcal{R}_K < 1 < \mathcal{R}_{K^*}$ – with such light masses it gives non-negligible contributions. Furthermore, in a full calculation the LFV constraints were violated. To conclude on this term, no further efforts were done to tune the parameters for a significant mixing.

For the third term, one can substitute the expression $2\sqrt{3} \tan \beta \lambda_4 / (3\lambda_6) \approx 1 + 8m_{R_2}^2 / (3\lambda_6 v_\chi^2)$ (see eq. 3.40) and split the fraction into

$$\frac{2\sqrt{3} \tan \beta \lambda_4}{3\lambda_6 (\tan^2 \beta + 1)} \approx \frac{1}{(\tan^2 \beta + 1)} + \frac{8m_{R_2}^2}{3\lambda_6 v_\chi^2 (\tan^2 \beta + 1)} \tag{4.5}$$

The second term is maximized e.g. with the choice $\lambda_6 = \frac{3}{8} \cdot 10^{-14}$, $m_{R_2} = 1500 \text{ GeV}$, and $\tan \beta = 0.1$. This would mean a value of $\alpha = 0.01 \text{ GeV}^2$ and therefore again all the leptoquarks being light. So, the discussion above holds again.

Altogether, the mixing matrix provides suppression with typical mixing not larger than 10^{-2} , except for singular points, which again are not of further interest for the purpose of explaining the anomalies.

4.3. Relevant NP calculations

The new particles extend severely the possible graphs for several observables. Calculations were done to determine the tree-level contributions for the anomalies $\mathcal{R}_{D^{(*)}}$ and $\mathcal{R}_{K^{(*)}}$ as well as the charged scalar gluon's contribution to $b \rightarrow s \gamma$.

4. Phenomenological considerations

4.3.1. Contribution of the scalar gluon G^+ to $b \rightarrow s \gamma$

All three scalar gluon contribute to the process $b \rightarrow s \gamma$, for the sake of simplicity only the one for the charged one has been computed. Furthermore, the approximation $m_b \gg m_s$ has been applied.

$$\begin{aligned} i\mathcal{M} = & \left[f_1(V_d^\dagger Y_2^* Y_2^T V_d) + f_2(U_d^\dagger Y_4^T Y_4^* U_d) - \right. \\ & \left. - f_3(V_d^\dagger Y_2^* U_u V_u^\dagger Y_4^* U_d) \right] im_b \frac{e}{8\pi^2} \mathcal{O}'_7 + \\ & + \left[f_1(U_d^\dagger Y_4^T Y_4^* U_d) + f_2(V_d^\dagger Y_2^* Y_2^T V_d) - \right. \\ & \left. - f_3(U_d^\dagger Y_4^T V_u U_u^\dagger Y_2^T V_d) \right] im_b \frac{e}{8\pi^2} \mathcal{O}_7 \quad , \end{aligned} \quad (4.6)$$

where $\mathcal{O}_7^{(\prime)}$ is defined in eq. 4.15 and the functions $f_{1,2,3}$ have been used, defined as

$$\begin{aligned} f_1 = & \frac{1}{m_b^2} \frac{1}{2(x-1)^2} (-1 + 4x - 3x^2 + 2x^2 \log x) + \\ & + \frac{1}{m_G^2} \frac{1}{54(x-1)^4} (5 - 27x + 27x^2 - 5x^3 + 6 \log x - 18x \log x) \end{aligned} \quad (4.7)$$

$$f_2 = \frac{1}{m_G^2} \frac{1}{54(x-1)^4} (11 - 18x + 9x^2 - 2x^3 + 6 \log x) \quad (4.8)$$

$$f_3 = \frac{m_q}{m_b m_G^2} \frac{2}{3(x-1)^2} (1 - x + \log x) \quad . \quad (4.9)$$

Here m_q denotes the mass of the up-type quark in the loop and the variable is $x = m_q^2/m_G^2$. The neutral scalar gluons contribute with terms of a similar structure to the ones above and there are contributions to the operator $\mathcal{O}_8 = (\bar{s}\sigma_{\mu\nu}P_R b)G^{\mu\nu}$, too. As the process was unexpectedly not of interest for constricting the parameter space, further calculations to this process were not done.

4.3.2. Tree-level contribution for $\mathcal{R}_{D^{(*)}}$

Regarding the corresponding tree-level graphs for $\mathcal{R}_{D^{(*)}}$, $b \rightarrow c l \nu_\alpha$, the process receives additional terms through R' and h^+ .

As discussed in chapter 3.3.4, it is possible to choose the charged Higgs' mass as high as necessary to avoid undesired effects in the observables. Furthermore, the mixing matrix Z^{LQ} provides no relevant mixing, consequently terms with e.g. $\sum_k Z_{1k}^{\text{LQ}} \cdot Z_{2k}^{\text{LQ}}$ are suppressed, see the previous section 4.2. Going on, decays with right-handed neutrinos as external states are also not to be considered because they are too heavy, thus kinematically inaccessible, and their mixing into the light-weighted neutrinos is negligible. Nevertheless, for the sake of completeness the full expressions can be found in appendix D.

As pointed out in sec. 3.3.4, always one of the representation of R' is light while the other one is heavy. It follows that in the sums over the leptoquark representations $R'_{(k)}$ only the term $k = 2$ has to be taken into account for an approximation. As a consequence, the only term of interest is

$$i\mathcal{M} = \frac{1}{2} \frac{|Z_{12}^{\text{LQ}}|^2}{m_{R'_{(2)}}^2} (Y_4^T V_d)_{i3} \cdot (U_u^\dagger Y_2^T U_{\nu,L})_{2\alpha} (\bar{c}_R b_L) (l_R \nu_{\alpha,L}) \quad (4.10)$$

where α and i is the index for the neutrino and charged lepton generation, respectively. However, Sakaki et al. [55] performed a fit of this operator to \mathcal{R}_D and \mathcal{R}_{D^*} . The result was a size of the couplings of approx. 2 for a mass $m_{R_2^{2/3}} = O(1 \text{ TeV})$. This fit also counts for the above formula for our representations and will be examined later-on in sec. 5.4.

4.3.3. Tree-level contribution for $\mathcal{R}_{K^{(*)}}$

Looking at the possible interactions, the B meson decay receives tree-level contributions by three of the scalar particles: the neutral Higgses h , the pseudo-scalar A , and the mixed scalar leptoquark R' .

Again, the whole expressions can be looked up in the appendix D.2. Because m_A and m_{h_2} can be chosen arbitrarily high and h_3 is heavy in any case, their corresponding terms are suppressed. It has been proven numerically that h_1 is not contributing. The leptoquark is left as the only particular exchange particle. The tensor term can also not be considered because it is suppressed by the absent mixing in Z^{LQ} . This is in agreement with Alonso, Grinstein, and Martin Camalich [56], and their statement that tensor operators cannot be generated within an effective theory.

The standard basis commonly used in literature is defined as follows [34]:

$$\mathcal{O}_7^{(l)} = (\bar{s} \sigma_{\mu\nu} P_{R(L)} b) F^{\mu\nu} \quad (4.11)$$

$$\mathcal{O}_{9,l} = (\bar{s} \gamma_\mu P_L b) (\bar{l} \gamma^\mu l) \quad (4.12)$$

$$\mathcal{O}_{10,l} = (\bar{s} \gamma_\mu P_L b) (\bar{l} \gamma^\mu \gamma^5 l) \quad (4.13)$$

$$\mathcal{O}'_{9,l} = (\bar{s} \gamma_\mu P_R b) (\bar{l} \gamma^\mu l) \quad (4.14)$$

$$\mathcal{O}'_{10,l} = (\bar{s} \gamma_\mu P_R b) (\bar{l} \gamma^\mu \gamma^5 l) \quad (4.15)$$

The primed operators are however strongly suppressed in the SM. The basis used in section 2.2 is connected with the standard one here by

$$\mathcal{O}_{b_L l_R} = (\bar{s} \gamma_\mu P_L b) (\bar{l} \gamma_\mu P_R l) = \frac{1}{2} (\mathcal{O}_{9,l} + \mathcal{O}_{10,l}) \quad (4.16)$$

$$\mathcal{O}_{b_R l_L} = (\bar{s} \gamma_\mu P_R b) (\bar{l} \gamma_\mu P_L l) = \frac{1}{2} (\mathcal{O}'_{9,l} - \mathcal{O}'_{10,l}) . \quad (4.17)$$

This means that the NP coefficients are pairwise (oppositely) equal:

4. Phenomenological considerations

$$C_{9,l}^{\text{NP}} = C_{10,l}^{\text{NP}} = \frac{1}{2}C_{b_L l_R}^{\text{NP}} = -\frac{1}{4} \sum_{k=2}^3 \frac{1}{m_{R'(k)}^2} |Z_{1k}^{\text{LQ}}|^2 (Y_4^T V_D)_{g3} (V_D^\dagger Y_4^*)_{2g} \quad (4.18)$$

$$C'_{9,l}{}^{\text{NP}} = -C'_{10,l}{}^{\text{NP}} = \frac{1}{2}C_{b_R l_L}^{\text{NP}} = -\frac{1}{4} \sum_{k=2}^3 \frac{1}{m_{R'(k)}^2} |Z_{2k}^{\text{LQ}}|^2 (Y_4^* U_D)_{g3} (U_d^\dagger Y_4^T)_{2g} \quad (4.19)$$

Here, g means the generation of the lepton l . This coincides with the necessity of effects in $\mathcal{R}_{K^{(*)}}$ being produced by the coefficients $C_9^{(l)}$ and $C_{10}^{(l)}$, as stated in [56].

5. Results

In this chapter the generated scans are presented together with the conclusions drawn from them. For this purpose first the setup is presented and then, step by step, reasonable choices shall be found for each of the input parameters: first for the ones that are not necessary for explaining the anomalies, then the ones relevant to $\mathcal{R}_{K^{(*)}}$ and $\mathcal{R}_{D^{(*)}}$.

Some scans use the choice $\theta_{12} = \pi/2$, $\theta_{13} = 0$ and $\theta_{23} = \pi/4$. Due to a stringent argumentation this choice can be only explained *a posteriori* in section 5.6. The same counts for the standard input that has been used for the scans: it also can be explained afterwards and are therefore presented not until eq. 5.3-5.7 in section 5.6.

5.1. The setup

The model had been implemented in **SARAH** to produce the necessary model files for **SPheno** [40, 41], used in version 3.3.8. For a compact and useful generation of data, an auxiliary program was written to automatically adjust the parameters to get a physically meaningful variation of variables. This means that the masses m_{R_2} and $m_A (\simeq m_{h^+})$ were input, as well as the angles and the phase of the quark mixing matrix V_d , see 3.17, $\tan \beta$ and Y_2 and Y_5 . v_χ was always set to $4 \cdot 10^6$ GeV in order to not come in conflict with the constraint of the Kaon decay, see [54] and chapter 3.3. The phase δ in V_d was set to zero because observables sensitive to the phase were not taken into account. If not stated differently, the angles were varied in the ranges $\theta_{12}, \theta_{23} \in [0, \pi/2]$ and $\theta_{13} \in [-\pi/2, \pi/2]$. In the chosen parametrization of eq. 3.17, these ranges already include all possible combinations of signs.

From the two input masses, corresponding scalar couplings $\lambda_{4,6}$ were calculated and λ_7 was adjusted to yield the correct mass of 125 GeV for the lightest Higgs. The other scalar couplings were set to 0.1. The whole input was inserted into a **LesHouches.in** file for **SPheno**. For the calculation of $\mathcal{R}_{K^{(*)}}$ and $\mathcal{R}_{D^{(*)}}$, the resulting coefficients were handed over to **flavio** [57], in version 0.28, using the interface format **WCxf** [58].

Several experimental values were already taken into account to constrict the parameter space. The calculation of the respective Branching Ratios (BRs) were done in **SPheno** and a list can be found in tab. 5.2. For still unmeasured decays the experimental limit for the BR was also taken as the acceptance threshold: any BR from the calculation larger than this limit was seen as a violation of this constraint.

For the measured decays, the experimental values and theoretical predictions [59–61] were compared. Because the theoretical uncertainties were smaller than the

5. Results

experimental ones, the latter were used to define the bin, in which the branching ratios were acceptable. SPheno also provides the ratio of the full branching ratio and the SM branching ratio. Any deviation of this ratio from 1 that was smaller than the relative experimental error at 1σ was accepted. For the used bins, see tab. 5.1.

These bounds are depicted in the graphs as red dashed lines.

Observable	relative error	bin for $\text{BR}/\text{BR}_{\text{SM}}$
$B_s^0 \rightarrow \mu\mu$	$0.7/3.1 = 23\%$	[0.77, 1.23]
$B \rightarrow X_s \gamma$	$1.1/3.1 = 35\%$	[0.65, 1.35]

Table 5.1.: Relative experimental errors [49] for measured decays and their bins in which a deviation from the SM prediction was acceptable.

In the input files the option was provided to switch the inclusion of particles in the loop calculations on and off. With this feature it was possible to determine which particles were responsible for certain effects.

Observable	experimental BR
$\mu^- \rightarrow e^- \gamma$	$< 4.2 \cdot 10^{-13}$
$\mu^- \rightarrow e^- e^+ e^-$	$< 1.0 \cdot 10^{-12}$
$\tau^- \rightarrow e^- \gamma$	$< 3.3 \cdot 10^{-8}$
$\tau^- \rightarrow \mu^- \gamma$	$< 4.4 \cdot 10^{-8}$
$\tau^- \rightarrow \mu^- \mu^+ \mu^-$	$< 2.1 \cdot 10^{-8}$
$K_L^0 \rightarrow e^\pm \mu^\mp$	$< 4.7 \cdot 10^{-12}$
$B \rightarrow X_s \nu \nu$	$< 6.4 \cdot 10^{-4}$
$B_s^0 \rightarrow ee$	$< 2.8 \cdot 10^{-7}$
$B_s^0 \rightarrow \mu\mu$	$(3.1 \pm 0.7) \cdot 10^{-9}$
$B \rightarrow X_s \gamma$	$(3.1 \pm 1.1) \cdot 10^{-4}$

Table 5.2.: Considered constraints, values taken from [49].

5.2. Scan over m_A

Knowing that the required effect is caused by the representation $(3, 2, 7/6)$, the other particles should be chosen very heavy in order to prevent avoidable violations and effects through other particles like the pseudo-scalar A and the charged Higgs h^\pm , which indeed can effect the constraints, e.g. $B_s \rightarrow ll$.

The necessary mass scale was determined by some sample scans, see figure 5.1. As a result, the masses were fixed on the range $m_A, m_{h^\pm} \geq 50$ TeV. For reasons of simplicity, the mass was set to 100 TeV for the following scans.

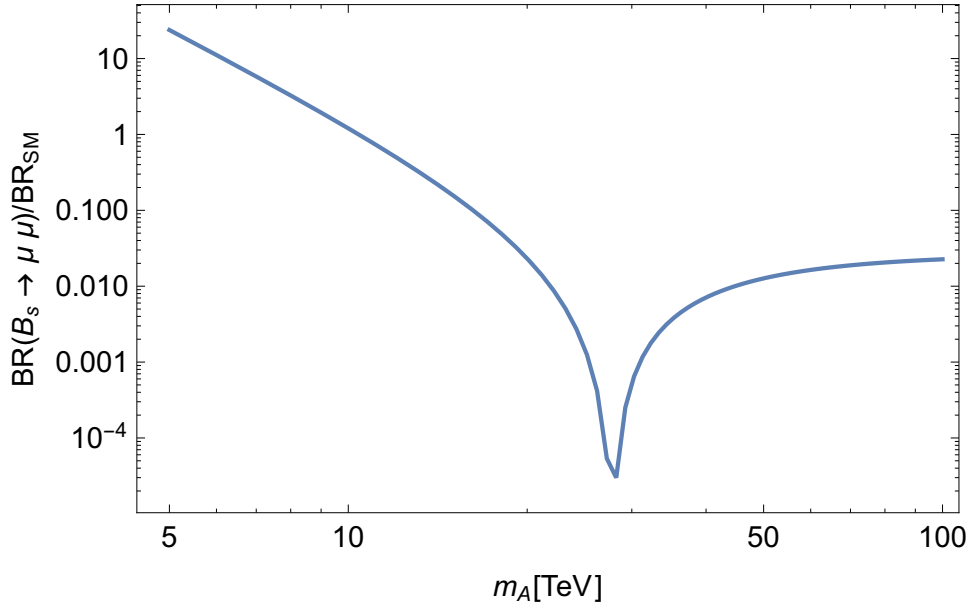


Figure 5.1.: Plot of $BR(B_s \rightarrow \mu^+ \mu^-)/BR_{SM}$ in dependence of m_A . The angles were chosen $\theta_{12} = \pi/2, \theta_{13} = 0, \theta_{23} = \pi/4$ and the leptoquark mass was set to $m_{R'_{(2)}} = 2$ TeV.

5.3. Input for Y_2 and Y_5

Having discussed the neutrino masses in chapter 3.2, it is known that the masses are determined by the input for Y_2 and Y_5 , which *a priori* is completely arbitrary as long as the neutrinos are too heavy to be observed.

This is however not the case. Scanning the parameter space, it is noticeable that the process $\mu \rightarrow e \gamma$ can receive severe contributions by $W^- - \nu$ - and $h^- - \nu$ -loops, as discussed in sec. 4.1 and see e.g. the graph in fig. 4.4. The same argumentation counts for $\tau \rightarrow \mu \gamma$ and $\tau \rightarrow e \gamma$.

The loop including h^- can be avoided by choosing a very high mass for this particle. On the other hand, this is not possible for the W boson. Thus, the Yukawa input had to be chosen large enough to get the new neutrinos heavy and suppress this contribution with the neutrino masses.

The matrix product $U_u^\dagger Y_2$ also couples $\bar{u}_R - R_2 - e_L$ interactions, and can enter the above process as displayed in fig. 4.5. This means that the coupling has to suppress these interactions, in order to not come in conflict with the constraints. Two plots of the branching ratios in dependence of the scale of Y_2 can be seen in fig. 5.2. There it is also visible that it would be in principle possible to achieve destructive interference between the terms $\propto Y_2$ and the other terms. This effect depends on the angles and would have to be fine-tuned for each choice of angles, though.

To simplify the matter, the matrices were chosen to be diagonal. The used values

5. Results

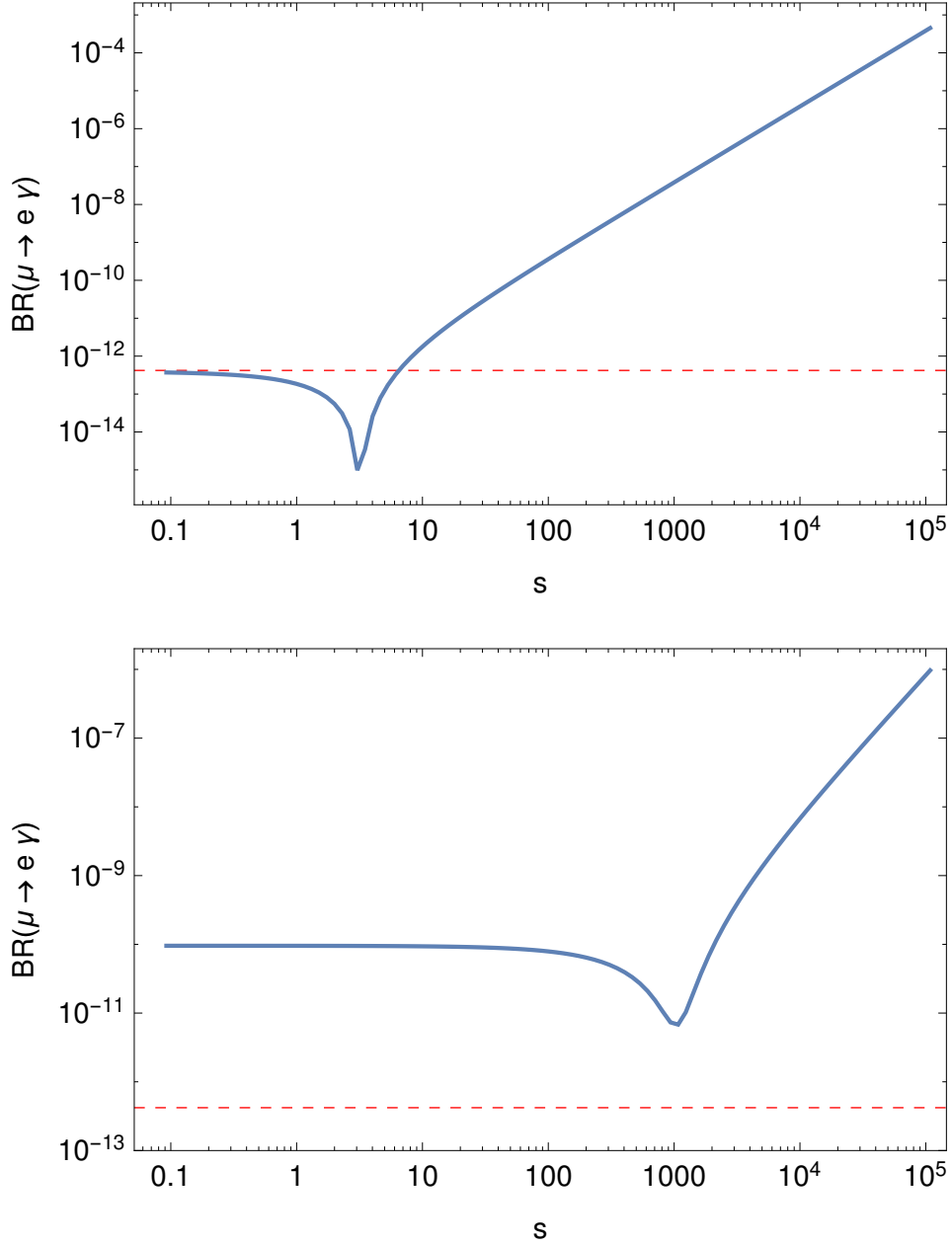


Figure 5.2.: Plot of $\text{BR}(\mu \rightarrow e \gamma)$ in a scan where Y_2 as defined in eq. 5.1 has been overall scaled with the factor s . The angles were chosen $\theta_{12} = \pi/2, \theta_{13} = 0, \theta_{23} = \pi/4$ for the upper scan and $\theta_{12}, \theta_{13}, \theta_{23} = 0.1$ for the lower. The leptoquark mass was $m_{R'_{(2)}} = 750$ GeV.

are

$$Y_2 = \text{diag}(10^{-8}, 10^{-7}, 10^{-5}) \quad \text{and} \quad Y_5 = \text{diag}(10^{-2}, 5 \cdot 10^{-2}, 10^{-1}) \quad (5.1)$$

where the hierarchy in the Y_2 is a compromise between the smallness of the entries and the mass hierarchy of the up-type quarks, in which this matrix enters. Y_5 is not further constrained and can be used to set the neutrino masses high enough. For the angles $\theta_{12} = \pi/2$, $\theta_{13} = 0$ and $\theta_{23} = \pi/4$ there is indeed destructive interference with these values for Y_2 as is visible in the upper plot in fig. 5.2.

These values in eq. 5.1 were used as input in all the scans, except for the one in the following chapter.

5.4. Results on $\mathcal{R}_{D^{(*)}}$

Regarding $\mathcal{R}_{D^{(*)}}$, the new contributions caused a deviation only of $O(10^{-5})$, which is still four orders of magnitude too small with respect to the anomalies in $\mathcal{R}_{D^{(*)}}$. The values obtained while scanning over $\tan\beta$ and the angles can be seen in fig. 5.3, in which the coupling Y_2 has been scaled up already by factor 100 compared to eq. 5.1 to magnify the effect. Re-examining the results in 4.3.2 and the previous section 5.3, one can now assess the coupling in eq. 4.10, a rough estimation gives an upper bound

$$(Y_4 V_d)_{g3} \cdot (U_u^\dagger Y_2 U_{\nu,L})_{2\alpha} < O(10^{-3}). \quad (5.2)$$

This is too small compared to the SM contribution to obtain any deviation from the prediction. The smallness is mainly driven by the violated LFV decays: They are increased with higher values for Y_2 and thus make it impossible to not suppress the respective couplings in the Wilson coefficients for $\mathcal{R}_{D^{(*)}}$. Therefore an explanation of $\mathcal{R}_{D^{(*)}}$ by this model can not be achieved.

5.5. Scans over $\tan\beta$ and $m_{R'_{(2)}}$

To fit $\mathcal{R}_{K^{(*)}}$, every value was accepted that lay within the 1σ range of the measurements, eq. 1.5. Therefore, the ranges $\mathcal{R}_K \in [0.648, 0.842]$ and $\mathcal{R}_{K^*} \in [0.57, 0.81]$ were considered.

For a first insight into the parameter space scans varying the three angles and $\tan\beta$ were done. As one can see in 5.4 the value of $\mathcal{R}_{K^{(*)}}$ depends stronger on $\tan\beta$ than on the three angles. As already has been pointed out, in the limit $\tan\beta \gg 1$, the coupling is enhanced $\propto \tan\beta$, which means that the associated effects get increased while contributions from the other two couplings, Y_1 and Y_3 will not be magnified, see eq. 3.14.

For a specific value of the leptoquark mass, one has to surpass a certain value of $\tan\beta$ to get a significant effect in the observable. This behaviour however can be easily understood as the New Physics contributions come into place with the

5. Results

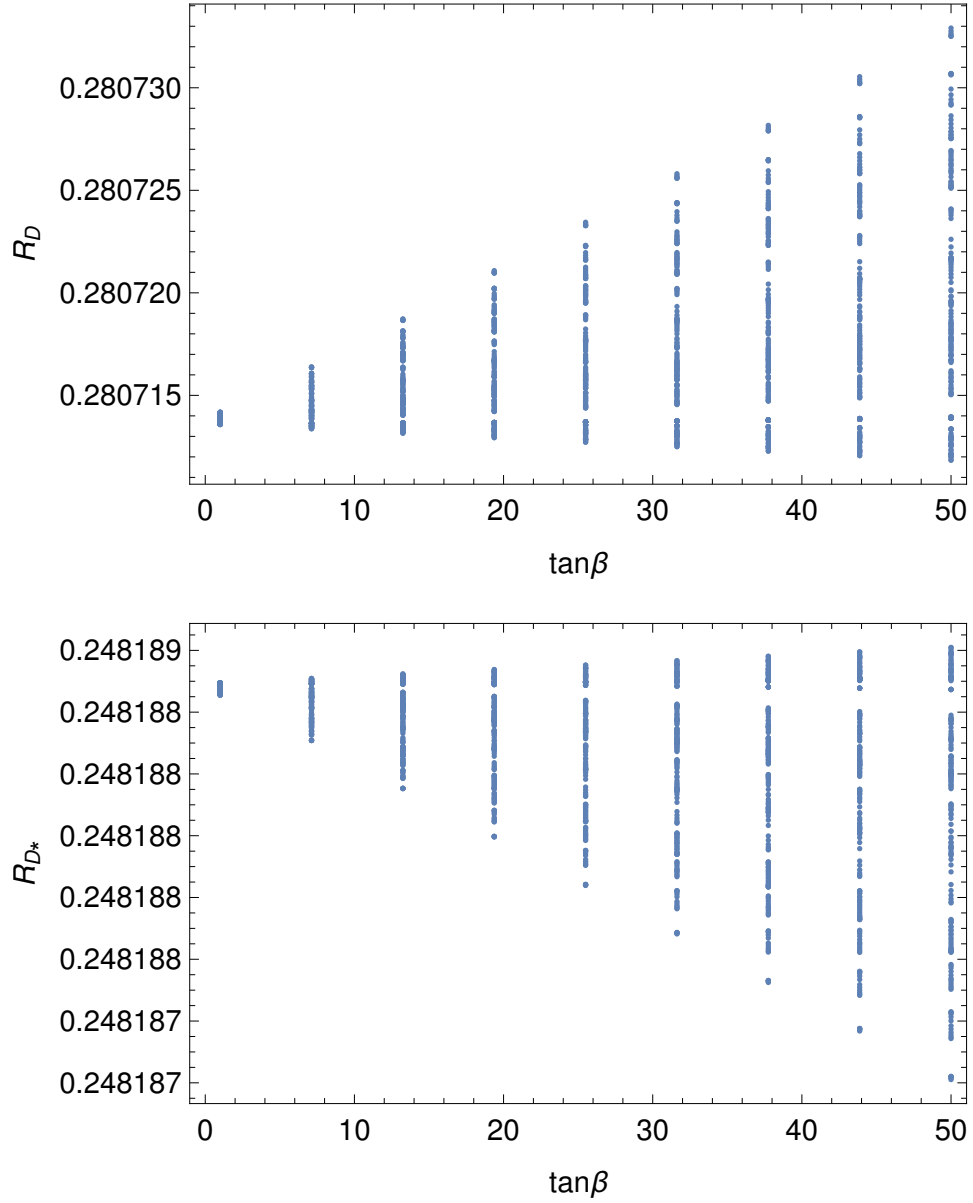


Figure 5.3.: Plots of \mathcal{R}_D (upper) and \mathcal{R}_{D^*} (lower), varying the angles θ_{kl} in 6 steps and $\tan\beta$ from 1 to 50 in 9 steps, with $m_{R'_{(2)}} = 750$ GeV and $m_A = 100$ TeV.

coupling $Y_4 \propto \tan \beta$ and it is visible to a fair extent in fig. 5.5, where the angles have been chosen to be $\theta_{12} = \pi/2, \theta_{13} = 0$ and $\theta_{23} = \pi/4$. This choice for the angles shall also be discussed in the next chapter.

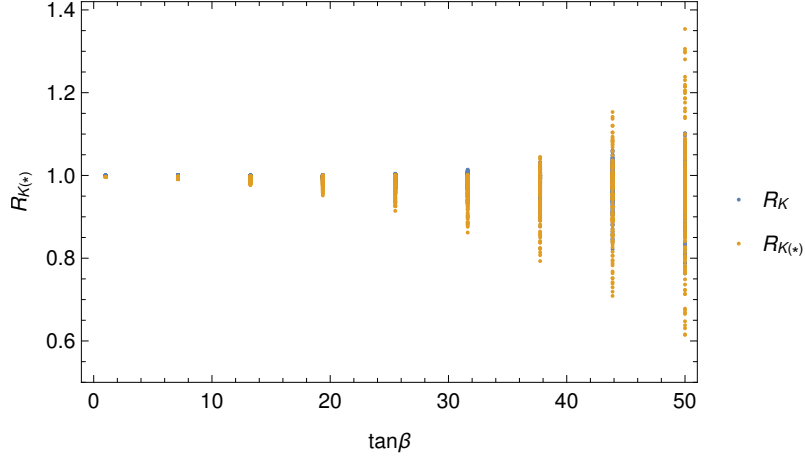


Figure 5.4.: Plot of $\mathcal{R}_{K^{(*)}}$, varying the angles θ_{kl} in 5 steps and $\tan \beta$ from 1 to 50 in 8 steps, with $m_{R'_{(2)}} = 750$ GeV and $m_A = 100$ TeV.

To conclude, $\tan \beta$ should be able to tune up the desired coupling without increasing the other ones, thus opening space for setting a higher mass and still obtaining a result within the bounds for $\mathcal{R}_{K^{(*)}}$. Regarding the mass of R' , with the maximal value $\tan \beta = 50$, one can still see effects in \mathcal{R}_K with $m_{R'_{(2)}} = 913$ TeV. A one-dimensional scan over the mass $m_{R'_{(2)}}$ for $m_A = m_{h^+} = 100$ TeV, $\tan \beta = 50$, $\theta_{12} = \pi/2$, $\theta_{13} = 0$ and $\theta_{23} = \pi/4$ can be seen in 5.6.

5.6. Scans over the angles' space

Up to here the sections provided an insight in how to choose the input parameters trying to explain the anomalies and avoiding violations of experimental bounds. The following standard input was used unless stated differently:

$$\tan \beta = 50 \quad (5.3)$$

$$m_A = m_{h^+} = 100 \text{ TeV} \quad (5.4)$$

$$Y_2 = \text{diag}(10^{-8}, 10^{-7}, 10^{-5}) \quad (5.5)$$

$$Y_5 = \text{diag}(10^{-2}, 5 \cdot 10^{-2}, 10^{-1}) \quad (5.6)$$

$$m_{R'_{(2)}} = 900 \text{ GeV} \quad (5.7)$$

The minima of \mathcal{R}_K and \mathcal{R}_{K^*} in the scans were both reached for the choice $\theta_{12} = \pi/2$, $\theta_{13} = 0$ and $\theta_{23} = \pi/4$, which is exactly the configuration that has been

5. Results

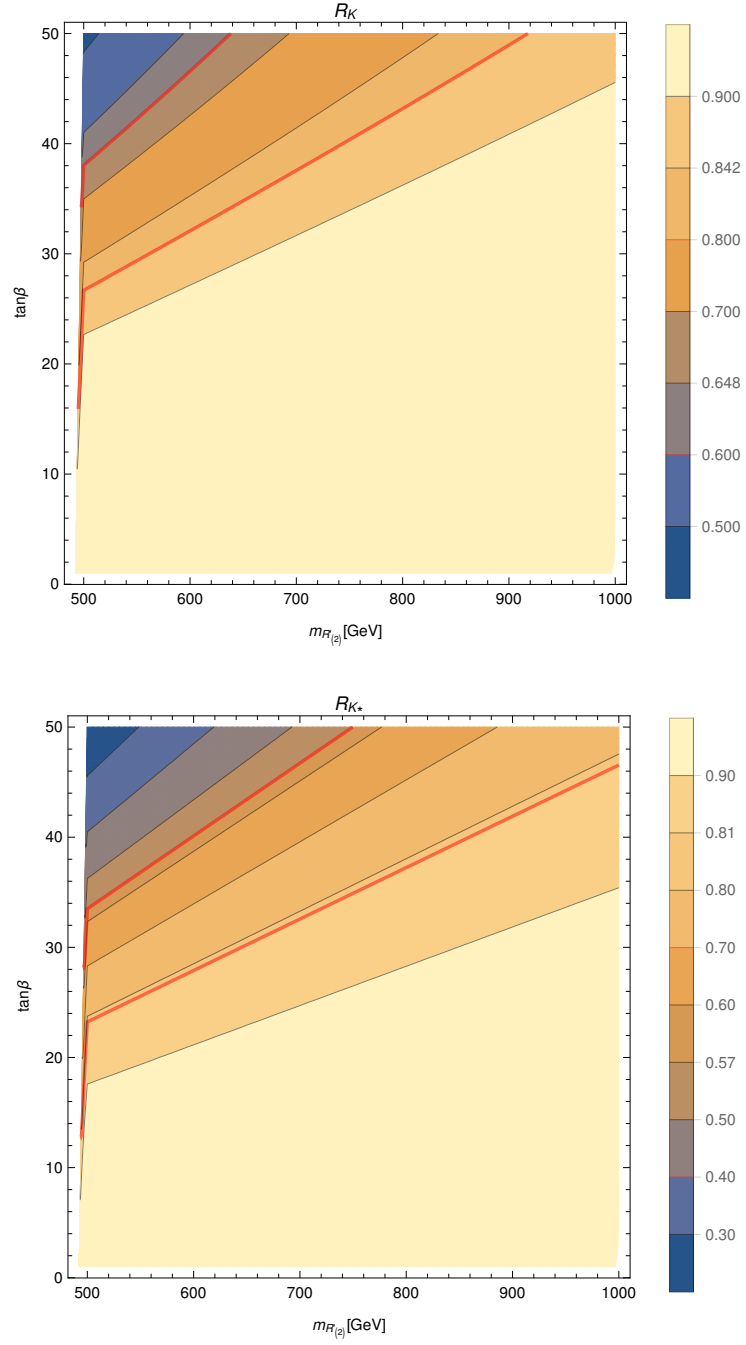


Figure 5.5.: Plot of \mathcal{R}_K (upper) and \mathcal{R}_{K^*} (lower), varying $m_{R'_{(2)}}$ and $\tan\beta$, with $(\theta_{12} = \pi/2, \theta_{13} = 0, \theta_{23} = \pi/4)$ and $m_A = 100$ TeV. The red lines mark the range within which the anomaly was considered to be explained.

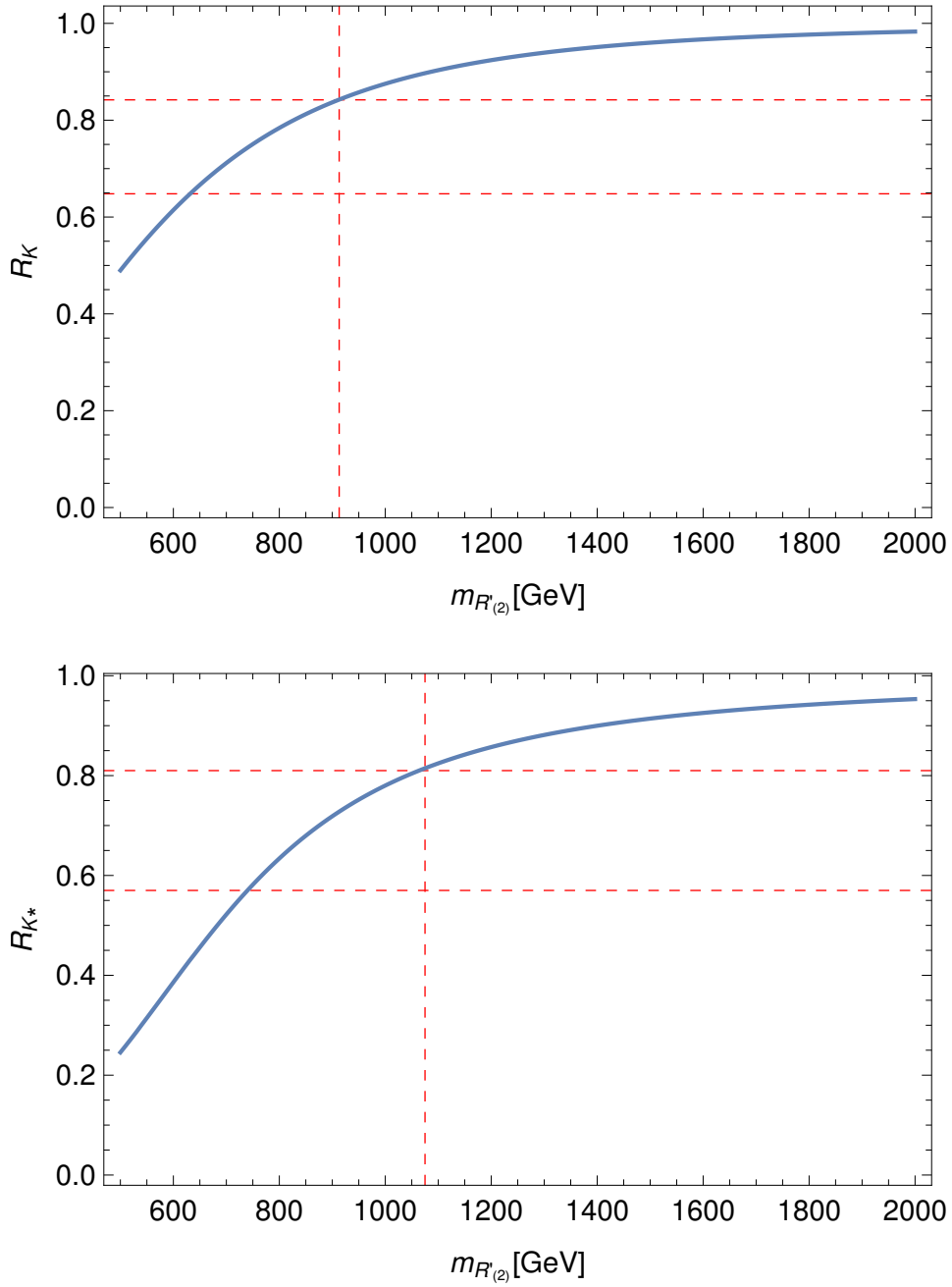


Figure 5.6.: Plot of \mathcal{R}_K (upper) and \mathcal{R}_{K^*} (lower) in dependence of $m_{R'_{(2)}}$, with $m_A = m_{h^+} = 100$ TeV, $\tan \beta = 50$, $\theta_{12} = \pi/2$, $\theta_{13} = 0$ and $\theta_{23} = \pi/4$. The lines mark the region wherein \mathcal{R}_K and \mathcal{R}_{K^*} are explained and the maximal mass for the leptoquark $R'_{(2)}$.

5. Results

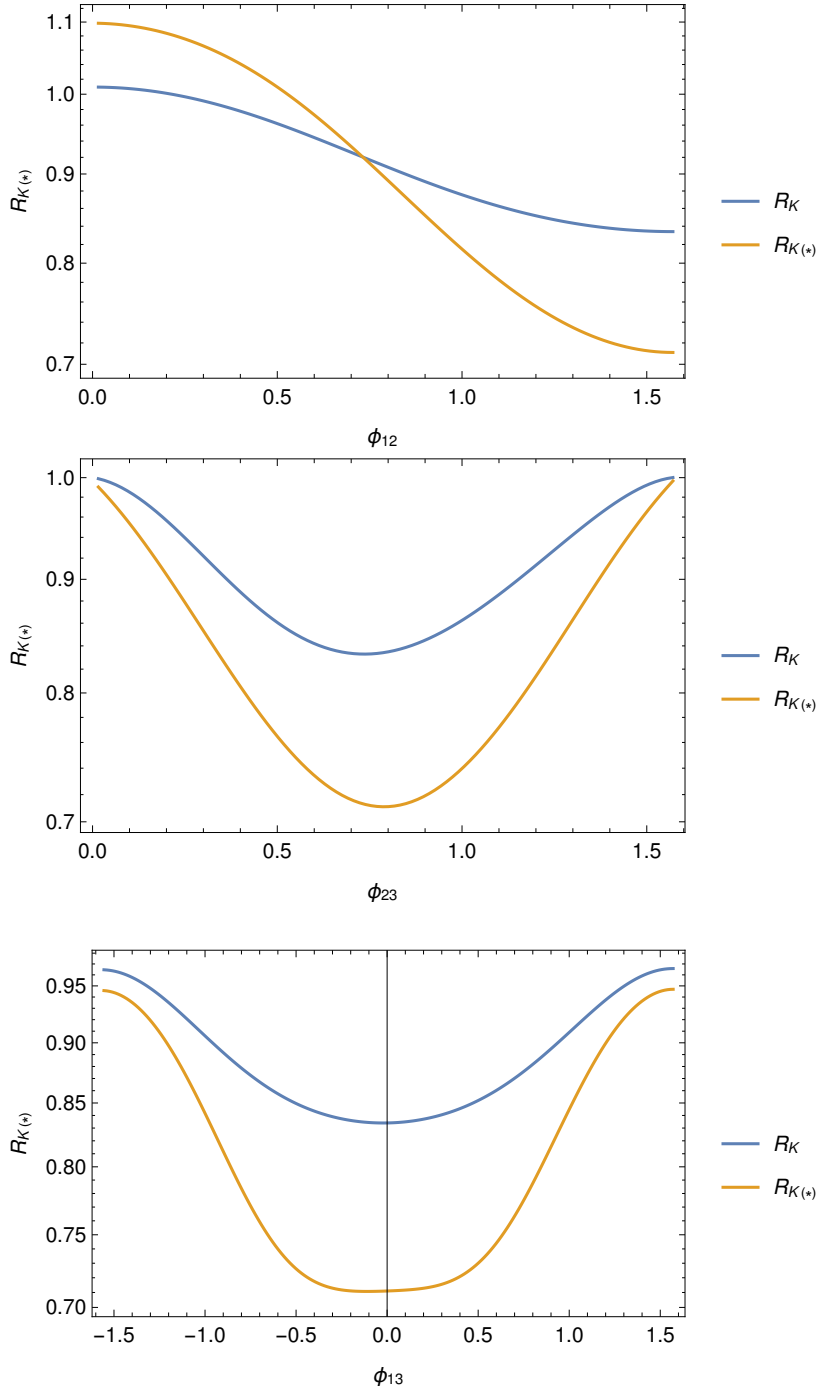


Figure 5.7.: Plots of \mathcal{R}_K and \mathcal{R}_{K^*} varying one angle θ_{kl} at a time, with $m_{R'_{(2)}} = 900$ GeV, $m_A = m_{h^+} = 100$ TeV, $\tan\beta = 50$ and $\theta_{12} = \pi/2$, $\theta_{13} = 0$ and $\theta_{23} = \pi/4$, respectively for the remaining angles.

used in some of the previous results. In one-dimensional scans it could be seen that it is not a singular point but rather a whole environment, that induces deviations in $\mathcal{R}_{K^{(*)}}$. The respective plots can be seen in 5.7.

Sensitive processes are the lepton flavour violating decays, which are plotted in fig. 5.8. Except for one point, it was not possible to determine a parameter combination that does not violate the process $\mu \rightarrow 3e$, while affecting \mathcal{R}_K . The process $\mu \rightarrow 3e$ is enhanced predominantly through the box-type diagrams.

The two light leptoquarks couple with the same matrix Y_4 as in the Wilson coefficient to $\mathcal{R}_{K^{(*)}}$. At the found minimum of \mathcal{R}_K , a **SPheno** calculation was done without R_2 and $R'_{(2)}$ loops and it indeed was seen that the violation comes due to the leptoquarks.

In fig. 5.9, one can see the observable $b \rightarrow s \gamma$, which is well within the bounds.

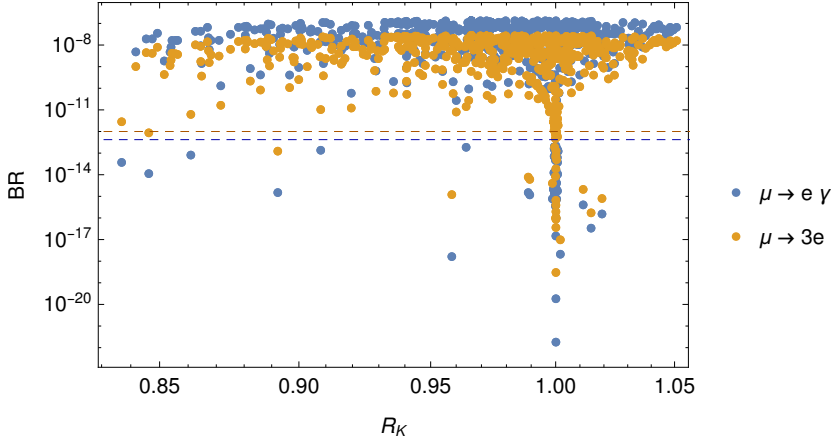


Figure 5.8.: Plot of $\text{BR}(\mu \rightarrow e \gamma)$ and $\text{BR}(\mu \rightarrow 3e)$ varying $\theta_{12}, \theta_{23} \in [0, \pi/2]$ in 8 steps and $\theta_{13} \in [-\pi/2, \pi/2]$ in 16 steps. The other parameters were $m_{R'_{(2)}} = 900$ GeV, $m_A = m_{h^+} = 100$ TeV and $\tan \beta = 50$. The dashed lines show the bounds for the respective decay. For $\text{BR}(\mu \rightarrow 3e)$ only one point is below the bound at $\mathcal{R}_K \approx 0.85$.

The most restricting process is the Kaon decay $K_L^0 \rightarrow e^\pm \mu^\mp$. This process is on quark-level the same as in $\mathcal{R}_{K^{(*)}}$, so this effect might be unavoidable. There were no points with $\mathcal{R}_K < 0.9$ found in which this process was not violated. The same counts for the measured decay of $B_s \rightarrow \mu^+ \mu^-$. A deviation of only 23% from the SM prediction is acceptable and for some singular points this bound was fulfilled. However, the calculations also showed deviations up to 1000% for otherwise interesting points with $\mathcal{R}_K < 0.9$.

The other considered constraints were not violated and the respective plots for these parameter scans can be seen in E. To conclude, the leptoquarks contribute in other leptonic observables and induce non-negligible effects on leptonic observables or leptonic meson decays. It is not possible to explain the measurement of $\mathcal{R}_{K^{(*)}}$ without violating experimental constraints within this model setup.

5. Results

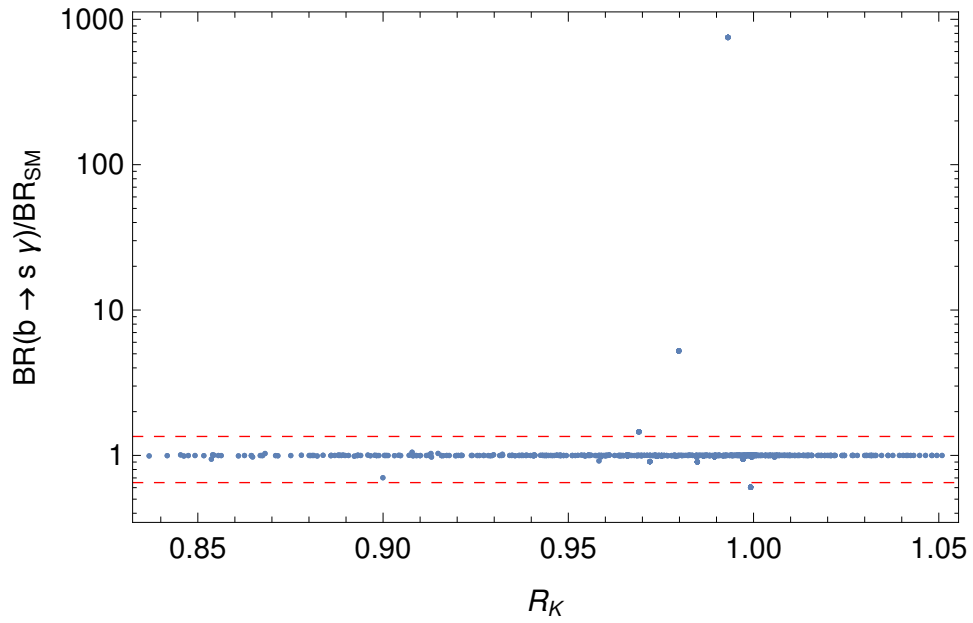


Figure 5.9.: Plot of $\text{BR}(b \rightarrow s \gamma)$ varying $\theta_{12}, \theta_{23} \in [0, \pi/2]$ in 8 steps and $\theta_{13} \in [-\pi/2, \pi/2]$ in 16 steps.

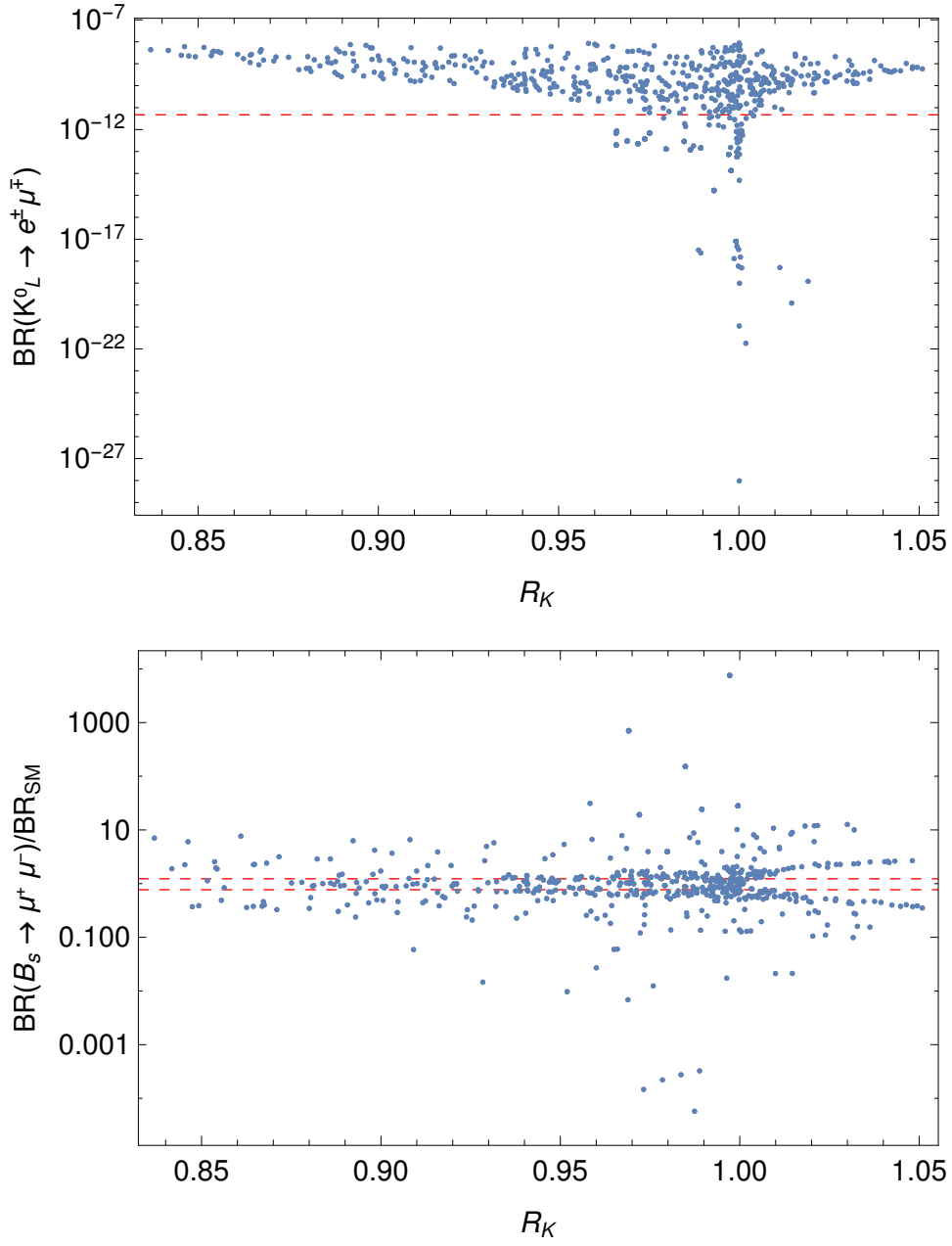


Figure 5.10.: Plot of $\text{BR}(K_L^0 \rightarrow e^\pm \mu^\mp)$ (upper) and $\text{BR}(B_s \rightarrow \mu^+ \mu^-)$ (lower), varying $\theta_{12}, \theta_{23} \in [0, \pi/2]$ in 8 steps and $\theta_{13} \in [-\pi/2, \pi/2]$ in 16 steps.

6. Conclusion and Outlook

Recent progress in the examinations at the collider experiments showed deviations from the Standard Model, that necessitate a deeper understanding of the physical constitution of the universe's particles. Additionally, a solution to these anomalies would at best also provide a unification of the forces and organize the leptons and the quarks in the same representation.

The model proposed by Fileviez Perez and Wise [1] would foremost solve the latter problem, providing a greater gauge group and the explanation, how the known gauge is established through symmetry breaking of a $SU(4)_C \otimes SU(2)_L \otimes U(1)_R$ gauge group, generating the fermionic sector in its known form.

Furthermore, chances were that the leptoquarks in this model could provide an explanation to the anomalous measurements of semileptonic observables. To achieve meaningful tests, the model had been implemented into **SARAH** and **SPheno** and the interesting observables were calculated with **flavio**. Efforts were made to understand the model's chances and drawbacks:

The mass structure was examined, indeed showing that two out of four leptoquarks might be light, one of which being reportedly able to explain the anomalies.

Unfortunately, the deviation in $\mathcal{R}_{D^{(*)}}$ was not tackled. The respective Wilson coefficients were too small to yield a deviation from the Standard Model coefficient, that would explain the anomaly. This was mainly driven by the necessity to choose small values for the coupling Y_2 that would have otherwise enhanced the branching ratios in lepton flavour violating decays, mainly $\mu \rightarrow e \gamma$ and $\mu \rightarrow 3e$.

It was possible to explain the measured values in the deviant observables \mathcal{R}_K and \mathcal{R}_{K^*} . On the other hand, this could be achieved only under the costs of violating constraints like $\mu \rightarrow e \gamma$ and $K_L^0 \rightarrow e^\pm \mu^\mp$, which made it in consequence impossible to hold on to the model in its first form.

However, one problem was that the proposed scalar potential was not the most general form. Some terms are missing and the respective couplings change the mass structure again. Certainly the scalar gluon does not have to be of the same mass as the light leptoquarks, in a full potential. Possibly, there could be a way to choose also the leptoquark R_2 heavy. Future work has to be done to recalculate the implications of the couplings that were not yet included in this work.

Looking forward, the violated constraints can be addressed by adding heavy leptons. This should lead to the freedom to minimize the problematic elements of the couplings that lead to the violation of the constraints. Currently, work is done to examine this possibility and to implement this extended lepton sector in an appropriate model in **SARAH** to obtain the necessary **SPheno** files.

Furthermore, efforts are made to implement appropriate searches. At experiments

6. Conclusion and Outlook

like the Large Hadron Collider one might be able to find hints and signatures of leptoquarks like lepton plus jet signals. These would certainly be a great step towards establishing an unification of the fermion representations.

Acknowledgements

Writing this thesis I'm much obliged to many people: first, I thank Werner Porod for accepting me for this thesis and for the many things I learned in working with him and his group. Thanks to Thomas Faber for patiently discussing questions with me and, together with Florian Staub, Helena Kolečová and Michal Malinský, for providing the **SARAH** model files. Thanks also to all the members of our working group for the kind atmosphere.

I also want to thank my friends who accompanied me throughout the studies, Alex, Michl, Max, Juli and Markus. There always was a inspiring discussion when we met for lunch.

And last but not least, I'm grateful for my parents and my siblings for always supporting me on my way.

A. The SU(4) generators

The basis of generators used to achieve the elements of the group are based on the so-called Gell-Mann matrices and extended to four dimensions. These matrices are not unique, so the choice shall be written explicitly here.

The basis has to consist of 15 matrices and the first are chosen to be the Gell-Mann matrices, see [62], embedded in 4×4 matrices and divided by two:

$$T_i = \frac{1}{2} \begin{pmatrix} \lambda_i & 0 \\ 0 & 0 \end{pmatrix}, \quad i = 1, \dots, 8 \quad (\text{A.1})$$

For the remaining seven matrices the following ones are used

$$\begin{aligned} T_9 &= \frac{1}{2} \begin{pmatrix} 0 & 0 & 0 & 1 \\ 0 & 0 & 0 & 0 \\ 0 & 0 & 0 & 0 \\ 1 & 0 & 0 & 0 \end{pmatrix}, & T_{10} &= \frac{1}{2} \begin{pmatrix} 0 & 0 & 0 & -i \\ 0 & 0 & 0 & 0 \\ 0 & 0 & 0 & 0 \\ i & 0 & 0 & 0 \end{pmatrix} \\ T_{11} &= \frac{1}{2} \begin{pmatrix} 0 & 0 & 0 & 0 \\ 0 & 0 & 0 & 1 \\ 0 & 0 & 0 & 0 \\ 0 & 1 & 0 & 0 \end{pmatrix}, & T_{12} &= \frac{1}{2} \begin{pmatrix} 0 & 0 & 0 & 0 \\ 0 & 0 & 0 & -i \\ 0 & 0 & 0 & 0 \\ 0 & i & 0 & 0 \end{pmatrix} \\ T_{13} &= \frac{1}{2} \begin{pmatrix} 0 & 0 & 0 & 0 \\ 0 & 0 & 0 & 0 \\ 0 & 0 & 0 & 1 \\ 0 & 0 & 1 & 0 \end{pmatrix}, & T_{14} &= \frac{1}{2} \begin{pmatrix} 0 & 0 & 0 & 0 \\ 0 & 0 & 0 & 0 \\ 0 & 0 & 0 & -i \\ 0 & 0 & i & 0 \end{pmatrix} \\ T_{15} &= \frac{1}{2\sqrt{6}} \begin{pmatrix} 1 & 0 & 0 & 0 \\ 0 & 1 & 0 & 0 \\ 0 & 0 & 1 & 0 \\ 0 & 0 & 0 & -3 \end{pmatrix} \end{aligned} \quad (\text{A.2})$$

This basis fulfils the relation

$$\text{Tr} [T_m T_n] = \frac{1}{2} \delta_{mn} . \quad (\text{A.3})$$

B. Fierz transformation

When working with leptoquark models, interactions come into place that are not present in the SM. They lead to bilinears that mix leptons and quarks and are hence not covered by standard basis, where only quark pairs or lepton pairs appear.

However, there is a transformation first introduced by Fierz [63], with which one can rearrange the bilinears and which shall be defined here. First, a shorthand notation is introduced, namely

$$\begin{aligned}
 \hat{s}(a, b; c, d) &= (ab)(cd) \\
 \hat{v}(a, b; c, d) &= (a\gamma_\mu b)(c\gamma^\mu d) \\
 \hat{t}(a, b; c, d) &= \frac{1}{2}(a\sigma_{\mu\nu}b)(c\sigma^{\mu\nu}d) \\
 \hat{a}(a, b; c, d) &= (a\gamma^5\gamma_\mu b)(c\gamma^\mu\gamma^5d) \\
 \hat{p}(a, b; c, d) &= (a\gamma^5b)(c\gamma^5d)
 \end{aligned} \tag{B.1}$$

where the function names stand for scalar, vector, tensor, axial, and pseudo-scalar type, respectively.

Combining the types to a vector to obtain a matrix equation, each of the bilinears can be expressed in a different basis by the transformation [62]

$$\begin{pmatrix} \hat{s} \\ \hat{v} \\ \hat{t} \\ \hat{a} \\ \hat{p} \end{pmatrix} (a, d; c, b) = \frac{1}{4} \begin{pmatrix} 1 & 1 & 1 & 1 & 1 \\ 4 & -2 & 0 & 2 & -4 \\ 6 & 0 & -1 & 0 & 6 \\ 4 & 2 & 0 & -2 & -4 \\ 1 & -1 & 1 & -1 & 1 \end{pmatrix} \begin{pmatrix} \hat{s} \\ \hat{v} \\ \hat{t} \\ \hat{a} \\ \hat{p} \end{pmatrix} (a, b; c, d) . \tag{B.2}$$

Generalized forms of this transformation with other permutations can be found in [64].

C. The Lagrangian, expanded and after EWSB

All products within eq. 3.8 are expanded and the particles transformed into mass basis. The resulting are written below. The summation convention counts. The equation has been split into parts of the Yukawa couplings, i.e. \mathcal{L}_n denotes the term proportional to Y_n .

$$\begin{aligned} \mathcal{L}_1 = & -\frac{1}{\sqrt{2}}\bar{u}_R U_u^\dagger Y_1^T V_u u_L (v_1 + Z_{1n}^h h_n + iZ_{13}^A A) + \bar{u}_R U_u^\dagger Y_1^T V_d d_L Z_{12}^{h^+} h^+ - \\ & -\frac{1}{\sqrt{2}}\bar{\nu} U_{\nu,R}^\dagger Y_1^T U_{\nu,L} \nu (v_1 + Z_{1i}^h h_i + iZ_{13}^A A) + \bar{\nu}_\alpha (U_{\nu,R}^\dagger Y_1^T) Z_{12}^{h^+} e_L h^+ + \text{h.c.} \end{aligned} \quad (\text{C.1})$$

$$\begin{aligned} \mathcal{L}_2 = & -\frac{1}{\sqrt{2}}\bar{u}_R U_u^\dagger Y_2^T V_u u_L (G_{(1)}^0 + iG_{(2)}^0) - \bar{u}_R U_u^\dagger Y_2^T U_{\nu,L} \nu Z_{1k}^{\text{LQ}} R'_{(k)} - \\ & -\bar{\nu} U_{\nu,R}^\dagger Y_2^T V_u Z_{2k}^{\text{LQ},*} R'_{(k)} u_L - \frac{1}{4\sqrt{3}}\bar{u}_R U_u^\dagger Y_2^T V_u (v_2 + Z_{3n}^h h_n + iZ_{33}^A A) u_L + \\ & + \sqrt{\frac{3}{4}}\bar{\nu} U_{\nu,R}^\dagger Y_2^T U_{\nu,L} \nu (v_2 + Z_{3n}^h h_n + iZ_{33}^A A) + \\ & + \bar{u}_R U_u^\dagger Y_2^T V_d d_L G^+ + \bar{u}_R U_u^\dagger Y_2^T R_2 e_L + \bar{\nu} U_{\nu,R}^\dagger Y_2^T V_d d_L \tilde{R}_2 + \\ & + \frac{1}{2\sqrt{6}}\bar{u}_R U_u^\dagger Y_2^T V_d d_L Z_{22}^{h^+} h^+ - \frac{3}{2\sqrt{6}}\bar{\nu} U_{\nu,R}^\dagger Y_2^T Z_{22}^{h^+} h^+ e_L + \text{h.c.} \end{aligned} \quad (\text{C.2})$$

$$\begin{aligned} \mathcal{L}_3 = & -\bar{d}_R U_d^\dagger Y_3^T V_u u_L Z_{12}^{h^+,*} h^- - \frac{1}{\sqrt{2}}\bar{d}_R U_d^\dagger Y_3^T V_d d_L (v_1 + Z_{1n}^h h_n - iZ_{13}^A A) - \\ & -\bar{e}_R Y_3^T U_{\nu,L} \nu Z_{12}^{h^+,*} h^- - \frac{1}{\sqrt{2}}\bar{e}_R Y_3^T e_L (v_1 + Z_{1n}^h h_n - iZ_{13}^A A) + \text{h.c.} \end{aligned} \quad (\text{C.3})$$

C. The Lagrangian, expanded and after EWSB

$$\begin{aligned}
\mathcal{L}_4 = & -\bar{d}_R U_d^\dagger Y_4^T V_u G^- u_L - \bar{d}_R U_d^\dagger Y_4^T U_{\nu,L\nu} \tilde{R}_2^* - \bar{e}_R Y_4^T V_u u_L R_2^* - \\
& -\frac{1}{2\sqrt{6}} \bar{d}_R U_d^\dagger Y_4^T V_u u_L Z_{22}^{h^+,*} h^- + \frac{3}{2\sqrt{6}} \bar{e}_R Y_4^T U_{\nu,L\nu} Z_{22}^{h^+,*} h^- - \\
& -\frac{1}{\sqrt{2}} \bar{d}_R U_d^\dagger Y_4^T V_d d_L (G_{(1)}^0 - iG_{(2)}^0) - \bar{d}_R U_d^\dagger Y_4^T e_L Z_{2k}^{\text{LQ}} R'_{(k)} - \\
& -\bar{e}_R Y_4^T V_d d_L Z_{1k}^{\text{LQ},*} R'_{(k)} - \frac{1}{4\sqrt{3}} \bar{d}_R U_d^\dagger Y_4^T V_d d_L (v_2 + Z_{3n}^h h_n - iZ_{33}^A A) + \\
& + \sqrt{\frac{3}{4}} \bar{e}_R Y_4^T e_L (v_2 + Z_{3n}^h h_n - iZ_{33}^A A) + \text{h.c.}
\end{aligned} \tag{C.4}$$

$$\begin{aligned}
\mathcal{L}_5 = & -\bar{u}_R U_u^\dagger Y_5^T U_{\nu,N\nu} Z_{3g}^{\text{LQ}} R'_{(g)} - \frac{1}{\sqrt{2}} \bar{\nu} U_{\nu,R}^\dagger U_{\nu,N\nu} (v_\chi + Z_{2n}^h h_n + iZ_{23}^A A) + \text{h.c.}
\end{aligned} \tag{C.5}$$

D. Wilson coefficients

All the calculated Wilson coefficients shall be presented here, the tree-level contributions to $b \rightarrow sl^+l^-$ and $\bar{b} \rightarrow \bar{c}l^+\nu$ and the G^- -loop contribution to $b \rightarrow s\gamma$. The definition of the mixing matrices $U_{u,d}$ and $V_{u,d}$ can be looked up in eq. 3.12.

D.1. $b \rightarrow s\gamma$

D.2. $b \rightarrow sl_i^+l_i^-$

The index i is not a summation index, but denotes the lepton generation. The used effective Hamiltonian and the operator basis is defined as

$$\begin{aligned} \mathcal{H}_{\text{eff}} = & C_T(\bar{s}_R\sigma^{\mu\nu}b_L)(\bar{l}_R\sigma_{\mu\nu}l_L) + C_{\text{SLL}}(\bar{s}_Rb_L)(\bar{l}_Rl_L) + C_{\text{SLR}}(\bar{s}_Rb_L)(\bar{l}_Ll_R) + \\ & + C_{\text{RR}}(\bar{s}_Lb_R)(\bar{l}_Ll_R) + C_{\text{SRL}}(\bar{s}_Lb_R)(\bar{l}_Rl_L) + C_{\text{VLR}}(\bar{s}_L\gamma^\mu b_L)(\bar{l}_R\gamma_\mu l_R) + \\ & + C_{\text{VRL}}(\bar{s}_R\gamma^\mu b_R)(\bar{l}_L\gamma_\mu l_L) + C_{\text{VLL}}(\bar{s}_L\gamma^\mu b_L)(\bar{l}_L\gamma_\mu l_L) \end{aligned} \quad (\text{D.1})$$

All of these coefficients except the last one receive contributions through the new particles. Their expressions are listed below.

D.2.1. Tensor operator

$$C_T^{\text{NP}} = - \sum_{k=2}^3 \frac{1}{8} \frac{1}{m_{R'_{(k)}}^2} Z_{1k}^{\text{LQ},*} (Y_4^T V_d)_{i3} (U_d^\dagger Y_4^T)_{2i} Z_{2k}^{\text{LQ}} \quad (\text{D.2})$$

D. Wilson coefficients

D.2.2. Scalar operators

$$b_L \rightarrow s_R l_L^+ l_R^-$$

$$\begin{aligned}
C_{\text{SLL}}^{\text{NP}} = & \left(\sum_{n=1}^3 \frac{1}{m_{h_n}^2} \left[\frac{\sqrt{3}}{12} Z_{3n}^h (U_d^\dagger Y_4^T V_d)_{23} + \frac{1}{\sqrt{2}} (U_d^\dagger Y_3^T V_d)_{23} Z_{1n}^h \right] \cdot \right. \\
& \cdot \left[\frac{\sqrt{3}}{4} Z_{3n}^h (Y_4^T)_{ii} - \frac{1}{\sqrt{2}} (Y_3^T)_{ii} Z_{1n}^h \right] - \\
& - \sum_{k=2}^3 \frac{1}{2} \frac{1}{m_{R'(k)}^2} Z_{1k}^{\text{LQ},*} (Y_4^T V_d)_{i3} (U_d^\dagger Y_4^T)_{2i} Z_{2k}^{\text{LQ}} + \\
& + \frac{1}{m_A^2} \left[\frac{\sqrt{3}}{12} Z_{33}^A (U_d^\dagger Y_4^T V_d)_{23} + \frac{1}{\sqrt{2}} (U_d^\dagger Y_3^T V_d)_{23} Z_{33}^A \right] \cdot \\
& \cdot \left. \left[-\frac{\sqrt{3}}{4} Z_{33}^A (Y_4^*)_{ii} + \frac{1}{\sqrt{2}} (Y_3^*)_{ii} Z_{33}^A \right] \right) \tag{D.3}
\end{aligned}$$

$$b_L \rightarrow s_R l_R^+ l_L^-$$

$$\begin{aligned}
C_{\text{SLR}}^{\text{NP}} = & \left(\sum_{n=1}^3 \frac{1}{m_{h_n}^2} \left[\frac{\sqrt{3}}{12} Z_{3n}^h (U_d^\dagger Y_4^T V_d)_{23} + \frac{1}{\sqrt{2}} (U_d^\dagger Y_3^T V_d)_{23} Z_{1n}^h \right] \cdot \right. \\
& \cdot \left[\frac{\sqrt{3}}{4} Z_{3n}^h (Y_4^*)_{ii} - \frac{1}{\sqrt{2}} (Y_3^*)_{ii} Z_{1n}^h \right] + \\
& + \frac{1}{m_A^2} \left[\frac{\sqrt{3}}{12} Z_{33}^A (U_d^\dagger Y_4^T V_d)_{23} + \frac{1}{\sqrt{2}} (U_d^\dagger Y_3^T V_d)_{23} Z_{33}^A \right] \cdot \\
& \cdot \left. \left[-\frac{\sqrt{3}}{4} Z_{33}^A (Y_4^*)_{ii} + \frac{1}{\sqrt{2}} (Y_3^*)_{ii} Z_{33}^A \right] \right) \tag{D.4}
\end{aligned}$$

$b_R \rightarrow s_L l_R^+ l_L^-$

$$\begin{aligned}
C_{RR}^{\text{NP}} = & \left(\sum_{n=1}^3 \frac{1}{m_{h_n}^2} \left[\frac{\sqrt{3}}{12} Z_{3n}^h (V_d^\dagger Y_4^* U_d)_{23} + \frac{1}{\sqrt{2}} (V_d^\dagger Y_3^* U_d)_{23} Z_{1n}^h \right] \cdot \right. \\
& \cdot \left[\frac{\sqrt{3}}{4} Z_{3n}^h (Y_4^*)_{ii} - \frac{1}{\sqrt{2}} (Y_3^*)_{ii} Z_{1n}^h \right] - \\
& - \sum_{k=2}^3 \frac{1}{2} \frac{1}{m_{R'(k)}^2} Z_{k2}^{\text{LQ},*} (Y_4^* U_d)_{i3} (V_d^\dagger Y_4^*)_{2i} Z_{1k}^{\text{LQ}} + \\
& + \frac{1}{m_A^2} \left[\frac{\sqrt{3}}{12} Z_{33}^A (V_d^\dagger Y_4^* U_d)_{23} + \frac{1}{\sqrt{2}} (V_d^\dagger Y_3^* U_d)_{23} Z_{13}^A \right] \cdot \\
& \cdot \left. \left[-\frac{\sqrt{3}}{4} Z_{33}^A (Y_4^*)_{ii} + \frac{1}{\sqrt{2}} (Y_3^*)_{ii} Z_{33}^A \right] \right) \quad (\text{D.5})
\end{aligned}$$

 $b_R \rightarrow s_L l_L^+ l_R^-$

$$\begin{aligned}
C_{SRL}^{\text{NP}} = & \left(\sum_{n=1}^3 \frac{1}{m_{h_n}^2} \left[\frac{\sqrt{3}}{12} Z_{3n}^h (V_d^\dagger Y_4^* U_d)_{23} + \frac{1}{\sqrt{2}} (V_d^\dagger Y_3^* U_d)_{23} Z_{1n}^h \right] \cdot \right. \\
& \cdot \left[\frac{\sqrt{3}}{4} Z_{n3}^h (Y_4^T)_{ii} - \frac{1}{\sqrt{2}} (Y_3^T)_{ii} Z_{n1}^h \right] + \\
& + \frac{1}{m_A^2} \left[\frac{\sqrt{3}}{12} Z_{33}^A (V_d^\dagger Y_4^* U_d)_{23} + \frac{1}{\sqrt{2}} (V_d^\dagger Y_3^* U_d)_{23} Z_{13}^A \right] \cdot \\
& \cdot \left. \left[-\frac{\sqrt{3}}{4} Z_{33}^A (Y_4^T)_{ii} + \frac{1}{\sqrt{2}} (Y_3^T)_{ii} Z_{33}^A \right] \right) \quad (\text{D.6})
\end{aligned}$$

D.2.3. Vector operators

$$\begin{aligned}
C_{VLR}^{\text{NP}} = & - \left(\sum_{k=2}^3 \frac{1}{2} \frac{1}{m_{R'(k)}^2} Z_{1k}^{\text{LQ},*} (Y_4^T V_d)_{i3} (V_d^\dagger Y_4^*)_{2i} Z_{1k}^{\text{LQ}} \right) \\
C_{VRL}^{\text{NP}} = & - \left(\sum_{k=2}^3 \frac{1}{2} \frac{1}{m_{R'(k)}^2} Z_{2k}^{\text{LQ},*} (Y_4^* U_d)_{i3} (U_d^\dagger Y_4^T)_{2i} Z_{2k}^{\text{LQ}} \right) \quad (\text{D.7})
\end{aligned}$$

D.2.4. Conversion to standard basis

It counts:

D. Wilson coefficients

$$\begin{aligned}
(\bar{s}_L \gamma^\mu b_L)(\bar{l}_R \gamma_\mu l_R) &= \frac{1}{2}(\mathcal{O}_{9,l} + \mathcal{O}_{10,l}) \\
(\bar{s}_R \gamma^\mu b_R)(\bar{l}_L \gamma_\mu l_L) &= \frac{1}{2}(\mathcal{O}'_{9,l} - \mathcal{O}'_{10,l})
\end{aligned} \tag{D.8}$$

Therefore the New Physics coefficients convert into the standard basis with

$$\frac{1}{2}C_{\text{VLR}}^{\text{NP}} = C_9^{\text{NP}} = C_{10}^{\text{NP}} \frac{1}{2}C_{\text{VRL}}^{\text{NP}} = C_9^{\text{NP}} = -C_{10}^{\text{NP}} \tag{D.9}$$

D.3. $\bar{b} \rightarrow \bar{c} l_i^+ \nu_\alpha$

The indices α and i used in this section denote the neutrino and lepton generation, respectively, and are not summation indices. The effective Hamiltonian is defined as

$$\begin{aligned}
\mathcal{H}_{\text{eff}} &= C_{\text{SRL}}(\bar{b}_L c_R)(\bar{\nu}_\alpha l_L) + C_{\text{SRR}}(\bar{b}_L c_R)(\bar{\nu}_\alpha l_R) + \\
&+ C_{\text{SLL}}(\bar{b}_R c_L)(\bar{\nu}_\alpha l_L) + C_{\text{SLR}}(\bar{b}_R c_L)(\bar{\nu}_\alpha l_R) + \\
&+ C_{\text{VLR}}(\bar{b}_L \gamma^\mu c_L)(\bar{\nu}_\alpha \gamma_\mu l_R) + C_{\text{VRL}}(\bar{b}_R \gamma^\mu c_R)(\bar{\nu}_\alpha \gamma_\mu l_L) + \\
&+ C_{\text{VLL}}^{\text{SM}}(\bar{b}_L \gamma^\mu c_L)(\bar{\nu}_\alpha \gamma_\mu l_L)
\end{aligned} \tag{D.10}$$

D.3.1. Scalar operators

$$\bar{b}_L \rightarrow \bar{c}_R l_L^+ \nu_\alpha$$

$$\begin{aligned}
C_{\text{SRL}}^{\text{NP}} &= \left(-\frac{1}{m_{h^+}^2} \left[Z_{12}^{h^+,*} (V_d^\dagger Y_1^* U_u)_{32} + \frac{1}{2\sqrt{6}} Z_{22}^{h^+,*} (V_d^\dagger Y_2^* U_u)_{32} \right] \cdot \right. \\
&\cdot \left[Z_{12}^{h^+} (U_{\nu,R}^\dagger Y_1^T)_{\alpha i} - \frac{3}{2\sqrt{6}} Z_{22}^{h^+} (U_{\nu,R}^\dagger Y_2^T)_{\alpha i} \right] + \\
&+ \sum_{k=2}^3 \frac{1}{2} \frac{1}{m_{R'(k)}^2} Z_{1k}^{\text{LQ}} (V_d^\dagger Y_4^*)_{3i} \cdot \\
&\cdot \left. \left[Z_{1k}^{\text{LQ},*} (U_{\nu,L}^\dagger Y_2^T U_u)_{\alpha 2} + Z_{3k}^{\text{LQ},*} (U_{\nu,N}^\dagger Y_5^T U_u)_{\alpha 2} \right] \right)
\end{aligned} \tag{D.11}$$

$$\bar{b}_L \rightarrow \bar{c}_R l_R^+ \nu_\alpha$$

$$\begin{aligned}
C_{\text{SRR}}^{\text{NP}} &= -\frac{1}{m_{h^+}^2} \left[Z_{12}^{h^+,*} (V_d^\dagger Y_1^* U_u)_{32} + \frac{1}{2\sqrt{6}} Z_{22}^{h^+,*} (V_d^\dagger Y_2^* U_u)_{32} \right] \cdot \\
&\cdot \left[-Z_{12}^{h^+} (U_{\nu,L}^\dagger Y_3^*)_{\alpha i} + \frac{3}{2\sqrt{6}} Z_{22}^{h^+} (U_{\nu,L}^\dagger Y_4^*)_{\alpha i} \right]
\end{aligned} \tag{D.12}$$

$$\bar{b}_R \rightarrow \bar{c}_L l_L^+ \nu_\alpha$$

$$C_{\text{SLL}}^{\text{NP}} = -\frac{1}{m_{h^+}^2} \left[-(U_d^\dagger Y_3^T V_u)_{32} Z_{12}^{h^+,*} - \frac{1}{2\sqrt{6}} (U_d^\dagger Y_4^T V_u)_{32} Z_{22}^{h^+,*} \right] \cdot \left[Z_{12}^{h^+} (U_{\nu,R}^\dagger Y_1^T)_{\alpha i} - \frac{3}{2\sqrt{6}} Z_{22}^{h^+} (U_{\nu,R}^\dagger Y_2^T)_{\alpha i} \right] \quad (\text{D.13})$$

$$\bar{b}_R \rightarrow \bar{c}_L l_R^+ \nu_\alpha$$

$$C_{\text{SLR}}^{\text{NP}} = \left(-\frac{1}{m_{h^+}^2} \left[-(U_d^\dagger Y_3^T V_u)_{32} Z_{12}^{h^+,*} - \frac{1}{2\sqrt{6}} (U_d^\dagger Y_4^T V_u)_{32} Z_{22}^{h^+,*} \right] \cdot \left[-Z_{12}^{h^+} (U_{\nu,L}^\dagger Y_3^*)_{\alpha i} + \frac{3}{2\sqrt{6}} Z_{22}^{h^+} (U_{\nu,L}^\dagger Y_4^*)_{\alpha i} \right] - \sum_{k=2}^3 \frac{1}{2} \frac{1}{m_{R'(k)}^2} \left| Z_{2k}^{\text{LQ}} \right|^2 (U_d^\dagger Y_4^T)_{3i} \cdot (U_{\nu,R}^\dagger Y_2^T V_u)_{\alpha 2} \right) \quad (\text{D.14})$$

D.3.2. Vector operators

$$C_{\text{VLR}}^{\text{NP}} = -\sum_{k=2}^3 \frac{1}{2} \frac{1}{m_{R'(k)}^2} Z_{1k}^{\text{LQ}} Z_{2k}^{\text{LQ},*} (V_d^\dagger Y_4^*)_{3i} \cdot (U_{\nu,R}^\dagger Y_2^T V_u)_{\alpha 2}$$

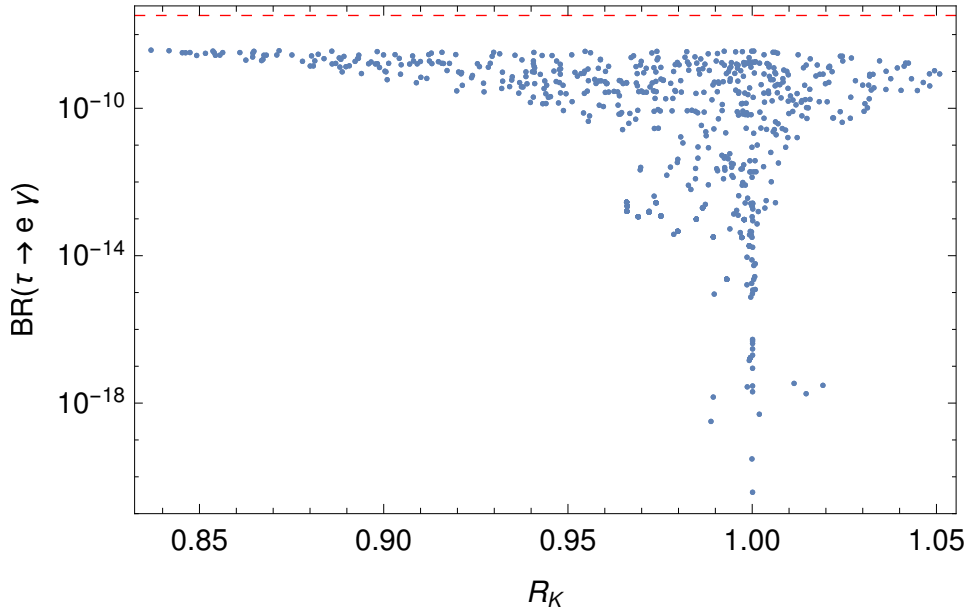
$$C_{\text{VRL}}^{\text{NP}} = -\sum_{k=2}^3 \frac{1}{2} \frac{1}{m_{R'(k)}^2} Z_{2g}^{\text{LQ}} (U_d^\dagger Y_4^T)_{3i} \left[(U_{\nu,L}^\dagger Y_2^* U_u)_{\alpha 2} Z_{1k}^{\text{LQ},*} + (U_{\nu,N}^\dagger Y_5^T U_u)_{\alpha 2} Z_{3k}^{\text{LQ},*} \right] \quad (\text{D.15})$$

E. Plots

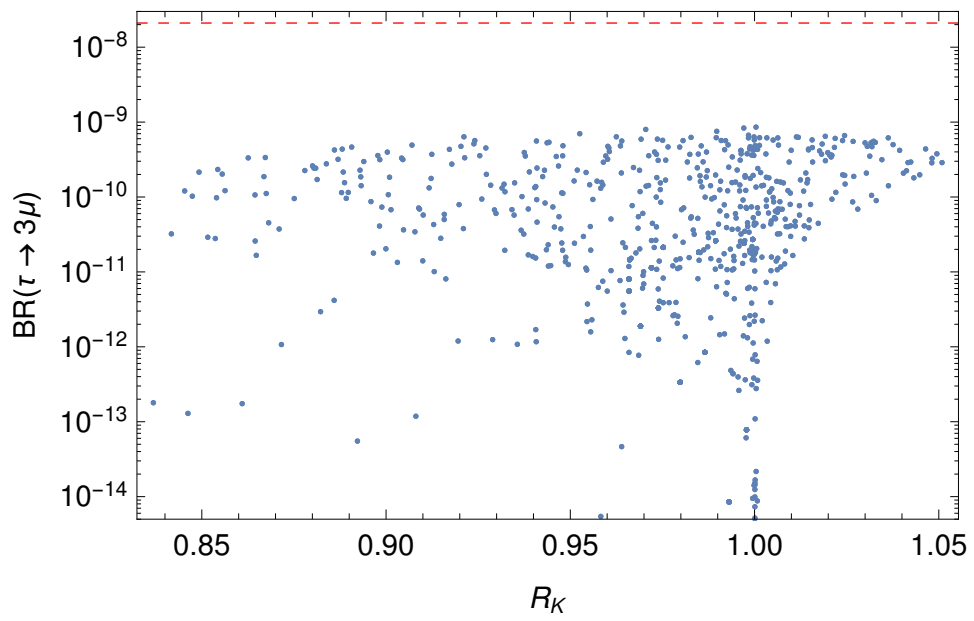
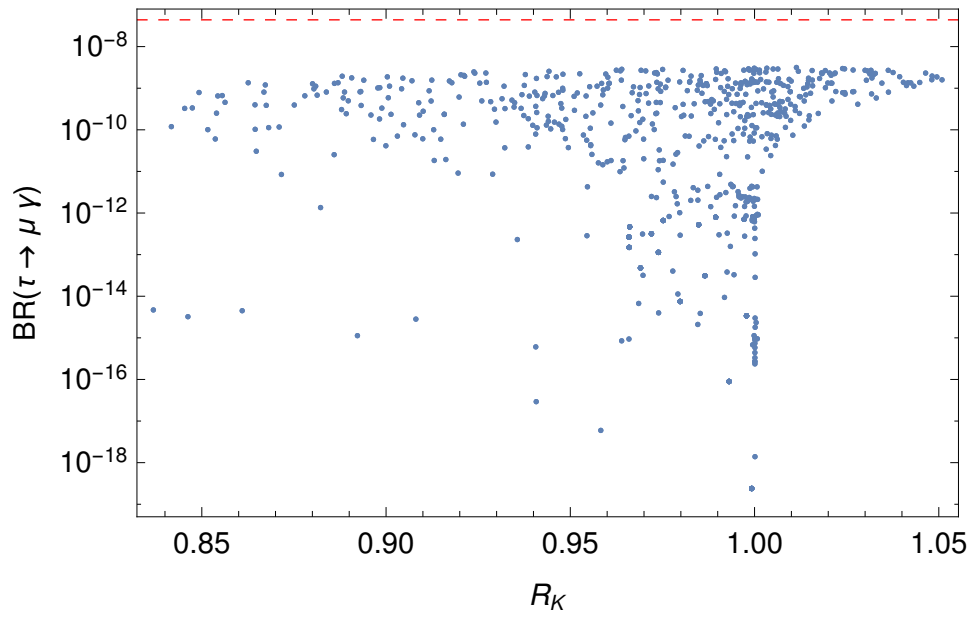
In this section the plots of the other observables are presented from a scan over the angles. In the scan $\theta_{12}, \theta_{23} \in [0, \pi/2]$ were varied in 8 steps and $\theta_{13} \in [-\pi/2, \pi/2]$ in 16 steps, while the phase $\delta = 0$.

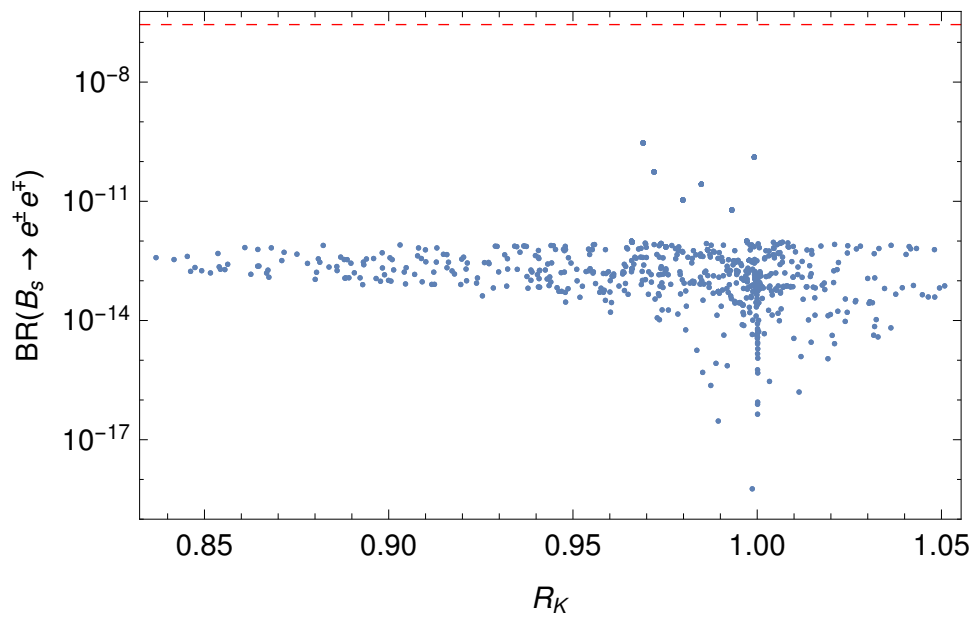
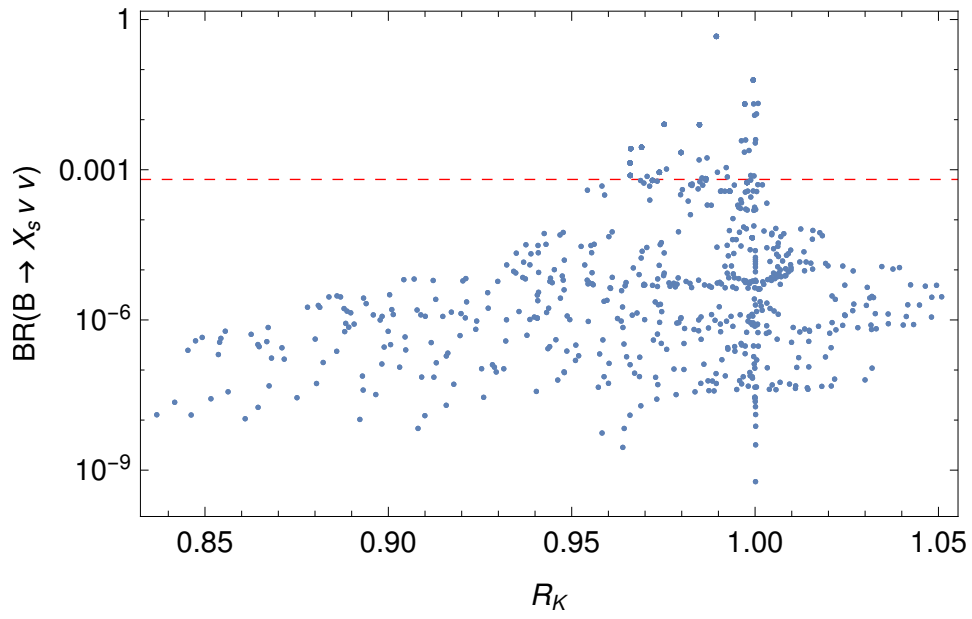
The masses were chosen to be $m_{R'_{(2)}} = m_{R_2} = 900$ GeV and $m_A = m_{h^+} = 100$ TeV, with $\tan \beta = 50$.

Each plot shows the branching ratio in dependence of \mathcal{R}_K . The red dashed lines show the bounds above which experimental constraints are violated, see tab. 5.2.



E. Plots





Bibliography

- [1] P. Fileviez Perez and M. B. Wise. “Low Scale Quark-Lepton Unification”. In: *Phys. Rev. D* 88 (2013), p. 057703. DOI: 10.1103/PhysRevD.88.057703. arXiv: 1307.6213 [hep-ph].
- [2] S. Weinberg. *The Quantum Theory of Fields. Foundations*. Vol. 1. Cambridge: Cambridge University Press, 1995. ISBN: 9780521670531. DOI: 10.1017/CB09781139644167.
- [3] M. Breidenbach et al. “Observed Behavior of Highly Inelastic Electron-Proton Scattering”. In: *Phys. Rev. Lett.* 23 (1969), pp. 935–939. DOI: 10.1103/PhysRevLett.23.935.
- [4] M. Gell-Mann. “A schematic model of baryons and mesons”. In: *Physics Letters* 8.3 (1964), pp. 214–215. ISSN: 0031-9163. DOI: [https://doi.org/10.1016/S0031-9163\(64\)92001-3](https://doi.org/10.1016/S0031-9163(64)92001-3). URL: <http://www.sciencedirect.com/science/article/pii/S0031916364920013>.
- [5] B. Björken and S. Glashow. “Elementary particles and SU(4)”. In: *Physics Letters* 11.3 (1964), pp. 255–257. ISSN: 0031-9163. DOI: [https://doi.org/10.1016/0031-9163\(64\)90433-0](https://doi.org/10.1016/0031-9163(64)90433-0). URL: <http://www.sciencedirect.com/science/article/pii/0031916364904330>.
- [6] M. Kobayashi and T. Maskawa. “CP-Violation in the Renormalizable Theory of Weak Interaction”. In: *Progress of Theoretical Physics* 49.2 (1973), pp. 652–657. DOI: 10.1143/PTP.49.652. URL: <http://dx.doi.org/10.1143/PTP.49.652>.
- [7] G. Aad et al. “Observation of a new particle in the search for the Standard Model Higgs boson with the ATLAS detector at the LHC”. In: *Phys. Lett. B* 716 (2012), pp. 1–29. DOI: 10.1016/j.physletb.2012.08.020. arXiv: 1207.7214 [hep-ex].
- [8] S. Chatrchyan et al. “Observation of a new boson at a mass of 125 GeV with the CMS experiment at the LHC”. In: *Phys. Lett. B* 716 (2012), pp. 30–61. DOI: 10.1016/j.physletb.2012.08.021. arXiv: 1207.7235 [hep-ex].
- [9] G. Ricciardi et al. “Flavour, Electroweak Symmetry Breaking and Dark Matter: state of the art and future prospects”. In: *Eur. Phys. J. Plus* 130.10 (2015), p. 209. DOI: 10.1140/epjp/i2015-15209-y. arXiv: 1507.05029 [hep-ph].
- [10] J. C. Pati and A. Salam. “Lepton Number as the Fourth Color”. In: *Phys. Rev. D* 10 (1974). [Erratum: *Phys. Rev. D* 11,703(1975)], pp. 275–289. DOI: 10.1103/PhysRevD.10.275, 10.1103/PhysRevD.11.703.2.

Bibliography

- [11] M. Bauer and M. Neubert. “Minimal Leptoquark Explanation for the $R_{D^{(*)}}$, R_K , and $(g - 2)_g$ Anomalies”. In: *Phys. Rev. Lett.* 116.14 (2016), p. 141802. DOI: 10.1103/PhysRevLett.116.141802. arXiv: 1511.01900 [hep-ph].
- [12] I. Doršner et al. “Can scalar leptoquarks explain the $f(D(s))$ puzzle?”. In: *Phys. Lett.* B682 (2009), pp. 67–73. DOI: 10.1016/j.physletb.2009.10.087. arXiv: 0906.5585 [hep-ph].
- [13] P. H. Frampton. “Light leptoquarks as possible signature of strong-electroweak unification”. In: *Modern Physics Letters A* 07.07 (1992), pp. 559–562. DOI: 10.1142/S0217732392000525.
- [14] H. Murayama and T. Yanagida. “Viable $SU(5)$ GUT with light leptoquark bosons”. In: *Modern Physics Letters A* 07.02 (1992), pp. 147–151. DOI: 10.1142/S0217732392000070.
- [15] I. Doršner. “Scalar leptoquark in $SU(5)$ ”. In: *Phys. Rev. D* 86 (5 Sept. 2012), p. 055009. DOI: 10.1103/PhysRevD.86.055009. URL: <https://link.aps.org/doi/10.1103/PhysRevD.86.055009>.
- [16] R. Barbieri, C. W. Murphy, and F. Senia. “B-decay Anomalies in a Composite Leptoquark Model”. In: *Eur. Phys. J.* C77.1 (2017), p. 8. DOI: 10.1140/epjc/s10052-016-4578-7. arXiv: 1611.04930 [hep-ph].
- [17] U. Aydemir et al. “B-decay anomalies and scalar leptoquarks in unified Pati-Salam models from noncommutative geometry”. In: (2018). arXiv: 1804.05844 [hep-ph].
- [18] A. M. Sirunyan et al. “Search for third-generation scalar leptoquarks decaying to a top quark and a τ lepton at $\sqrt{s} = 13$ TeV”. In: (2018). arXiv: 1803.02864 [hep-ex].
- [19] T. Blake, G. Lanfranchi, and D. M. Straub. “Rare B Decays as Tests of the Standard Model”. In: *Prog. Part. Nucl. Phys.* 92 (2017), pp. 50–91. DOI: 10.1016/j.pnpnp.2016.10.001. arXiv: 1606.00916 [hep-ph].
- [20] S. L. Glashow, J. Iliopoulos, and L. Maiani. “Weak Interactions with Lepton-Hadron Symmetry”. In: *Phys. Rev. D* 2 (7 Oct. 1970), pp. 1285–1292. DOI: 10.1103/PhysRevD.2.1285. URL: <https://link.aps.org/doi/10.1103/PhysRevD.2.1285>.
- [21] G. Degrandi, P. Gambino, and G. F. Giudice. “ $B \rightarrow X(s \gamma)$ in supersymmetry: Large contributions beyond the leading order”. In: *JHEP* 12 (2000), p. 009. DOI: 10.1088/1126-6708/2000/12/009. arXiv: hep-ph/0009337 [hep-ph].
- [22] J. P. Lees et al. “Evidence for an excess of $\bar{B} \rightarrow D^{(*)} \tau^- \bar{\nu}_\tau$ decays”. In: *Phys. Rev. Lett.* 109 (2012), p. 101802. DOI: 10.1103/PhysRevLett.109.101802. arXiv: 1205.5442 [hep-ex].

- [23] J. P. Lees et al. “Measurement of an Excess of $\bar{B} \rightarrow D^{(*)}\tau^{-}\bar{\nu}_{\tau}$ Decays and Implications for Charged Higgs Bosons”. In: *Phys. Rev. D* 88.7 (2013), p. 072012. DOI: 10.1103/PhysRevD.88.072012. arXiv: 1303.0571 [hep-ex].
- [24] M. Huschle et al. “Measurement of the branching ratio of $\bar{B} \rightarrow D^{(*)}\tau^{-}\bar{\nu}_{\tau}$ relative to $\bar{B} \rightarrow D^{(*)}\ell^{-}\bar{\nu}_{\ell}$ decays with hadronic tagging at Belle”. In: *Phys. Rev. D* 92.7 (2015), p. 072014. DOI: 10.1103/PhysRevD.92.072014. arXiv: 1507.03233 [hep-ex].
- [25] Y. Sato et al. “Measurement of the branching ratio of $\bar{B}^0 \rightarrow D^{*+}\tau^{-}\bar{\nu}_{\tau}$ relative to $\bar{B}^0 \rightarrow D^{*+}\ell^{-}\bar{\nu}_{\ell}$ decays with a semileptonic tagging method”. In: *Phys. Rev. D* 94.7 (2016), p. 072007. DOI: 10.1103/PhysRevD.94.072007. arXiv: 1607.07923 [hep-ex].
- [26] S. Hirose et al. “Measurement of the τ lepton polarization and $R(D^*)$ in the decay $\bar{B} \rightarrow D^*\tau^{-}\bar{\nu}_{\tau}$ ”. In: *Phys. Rev. Lett.* 118.21 (2017), p. 211801. DOI: 10.1103/PhysRevLett.118.211801. arXiv: 1612.00529 [hep-ex].
- [27] R. Aaij et al. “Measurement of the ratio of branching fractions $\mathcal{B}(\bar{B}^0 \rightarrow D^{*+}\tau^{-}\bar{\nu}_{\tau})/\mathcal{B}(\bar{B}^0 \rightarrow D^{*+}\mu^{-}\bar{\nu}_{\mu})$ ”. In: *Phys. Rev. Lett.* 115.11 (2015). [Erratum: *Phys. Rev. Lett.* 115, no. 15, 159901 (2015)], p. 111803. DOI: 10.1103/PhysRevLett.115.159901, 10.1103/PhysRevLett.115.111803. arXiv: 1506.08614 [hep-ex].
- [28] G. Wormser. $B^- \rightarrow D^{(*)}\tau\nu$ overview. URL: <https://indico.cern.ch/event/586719/contributions/2531261/> (visited on 03/26/2018).
- [29] Heavy Flavor Averaging Group. *Average of $R(D)$ and $R(D^*)$ for FPCP 2017*. URL: <http://www.slac.stanford.edu/xorg/hfag/semi/fpcp17/RDRDs.html> (visited on 03/26/2018).
- [30] S. Aoki et al. “Review of lattice results concerning low-energy particle physics”. In: *Eur. Phys. J. C* 77.2 (2017), p. 112. DOI: 10.1140/epjc/s10052-016-4509-7. arXiv: 1607.00299 [hep-lat].
- [31] S. Fajfer, J. F. Kamenik, and I. Nišandžić. “On the $B \rightarrow D^*\tau\bar{\nu}_{\tau}$ Sensitivity to New Physics”. In: *Phys. Rev. D* 85 (2012), p. 094025. DOI: 10.1103/PhysRevD.85.094025. arXiv: 1203.2654 [hep-ph].
- [32] R. Aaij et al. “Test of lepton universality using $B^+ \rightarrow K^+\ell^+\ell^-$ decays”. In: *Phys. Rev. Lett.* 113 (2014), p. 151601. DOI: 10.1103/PhysRevLett.113.151601. arXiv: 1406.6482 [hep-ex].
- [33] A. J. Buras. “Flavor dynamics: CP violation and rare decays”. In: *Subnucl. Ser.* 38 (2002), pp. 200–337. arXiv: hep-ph/0101336 [hep-ph].
- [34] M. Blanke. “Introduction to Flavour Physics and CP Violation”. In: *Proceedings, 2016 European School of High-Energy Physics (ESHEP2016): Skeikampen, Norway, June 15-28 2016*. 2017, pp. 71–100. arXiv: 1704.03753 [hep-ph]. URL: <https://inspirehep.net/record/1591344/files/arXiv:1704.03753.pdf>.

Bibliography

- [35] R. Aaij et al. “Test of lepton universality with $B^0 \rightarrow K^{*0} \ell^+ \ell^-$ decays”. In: *JHEP* 08 (2017), p. 055. DOI: 10.1007/JHEP08(2017)055. arXiv: 1705.05802 [hep-ex].
- [36] F. Staub. “From Superpotential to Model Files for FeynArts and CalcHep/CompHep”. In: *Comput. Phys. Commun.* 181 (2010), pp. 1077–1086. DOI: 10.1016/j.cpc.2010.01.011. arXiv: 0909.2863 [hep-ph].
- [37] F. Staub. “Automatic Calculation of supersymmetric Renormalization Group Equations and Self Energies”. In: *Comput. Phys. Commun.* 182 (2011), pp. 808–833. DOI: 10.1016/j.cpc.2010.11.030. arXiv: 1002.0840 [hep-ph].
- [38] F. Staub. “SARAH 3.2: Dirac Gauginos, UFO output, and more”. In: *Comput. Phys. Commun.* 184 (2013), pp. 1792–1809. DOI: 10.1016/j.cpc.2013.02.019. arXiv: 1207.0906 [hep-ph].
- [39] F. Staub. “SARAH 4 : A tool for (not only SUSY) model builders”. In: *Comput. Phys. Commun.* 185 (2014), pp. 1773–1790. DOI: 10.1016/j.cpc.2014.02.018. arXiv: 1309.7223 [hep-ph].
- [40] W. Porod. “SPHeno, a program for calculating supersymmetric spectra, SUSY particle decays and SUSY particle production at e^+e^- colliders”. In: *Comput. Phys. Commun.* 153 (2003), pp. 275–315. DOI: 10.1016/S0010-4655(03)00222-4. arXiv: hep-ph/0301101 [hep-ph].
- [41] W. Porod and F. Staub. “SPHeno 3.1: Extensions including flavour, CP-phases and models beyond the MSSM”. In: *Comput. Phys. Commun.* 183 (2012), pp. 2458–2469. DOI: 10.1016/j.cpc.2012.05.021. arXiv: 1104.1573 [hep-ph].
- [42] K. G. Wilson. “Non-Lagrangian Models of Current Algebra”. In: *Phys. Rev.* 179 (5 Mar. 1969), pp. 1499–1512. DOI: 10.1103/PhysRev.179.1499. URL: <https://link.aps.org/doi/10.1103/PhysRev.179.1499>.
- [43] K. G. Wilson and W. Zimmermann. “Operator product expansions and composite field operators in the general framework of quantum field theory”. In: *Communications in Mathematical Physics* 24.2 (June 1972), pp. 87–106. ISSN: 1432-0916. DOI: 10.1007/BF01878448. URL: <https://doi.org/10.1007/BF01878448>.
- [44] A. J. Buras. “Weak Hamiltonian, CP violation and rare decays”. In: *Probing the standard model of particle interactions. Proceedings, Summer School in Theoretical Physics, NATO Advanced Study Institute, 68th session, Les Houches, France, July 28-September 5, 1997. Pt. 1, 2.* 1998, pp. 281–539. arXiv: hep-ph/9806471 [hep-ph].
- [45] G. D’Amico et al. “Flavour anomalies after the R_{K^*} measurement”. In: *JHEP* 09 (2017), p. 010. DOI: 10.1007/JHEP09(2017)010. arXiv: 1704.05438 [hep-ph].

- [46] G. Hiller and I. Nišandžić. “ R_K and R_{K^*} beyond the standard model”. In: *Phys. Rev. D* 96 (3 Aug. 2017), p. 035003. DOI: 10.1103/PhysRevD.96.035003. URL: <https://link.aps.org/doi/10.1103/PhysRevD.96.035003>.
- [47] A. Crivellin et al. “Correlating lepton flavor universality violation in B decays with $\mu \rightarrow e\gamma$ using leptoquarks”. In: *Phys. Rev. D* 97.1 (2018), p. 015019. DOI: 10.1103/PhysRevD.97.015019. arXiv: 1706.08511 [hep-ph].
- [48] B. Bhattacharya et al. “Simultaneous Explanation of the R_K and $R(D^{(*)})$ Puzzles”. In: *Phys. Lett.* B742 (2015), pp. 370–374. DOI: 10.1016/j.physletb.2015.02.011. arXiv: 1412.7164 [hep-ph].
- [49] C. Patrignani et al. “Review of Particle Physics”. In: *Chin. Phys.* C40.10 (2016), p. 100001. DOI: 10.1088/1674-1137/40/10/100001.
- [50] I. Doršner et al. “Physics of leptoquarks in precision experiments and at particle colliders”. In: *Phys. Rept.* 641 (2016), pp. 1–68. DOI: 10.1016/j.physrep.2016.06.001. arXiv: 1603.04993 [hep-ph].
- [51] J. M. Arnold, B. Fornal, and M. B. Wise. “Phenomenology of scalar leptoquarks”. In: *Phys. Rev. D* 88 (2013), p. 035009. DOI: 10.1103/PhysRevD.88.035009. arXiv: 1304.6119 [hep-ph].
- [52] T. Faber, P. Meinzinger, W. Porod, F. Staub, H. Kolečová, M. Hudec and M. Malinský. *TBA*. 2018. In preparation.
- [53] P. Rösch. “SU(4), Leptoquarks und Neutrinos”. Bachelor thesis. University of Würzburg, 2016.
- [54] P. Stephan. “Beiträge von Vektor-Leptoquarks zu Kaonzerfällen”. Bachelor thesis. University of Würzburg, 2017.
- [55] Y. Sakaki et al. “Testing leptoquark models in $\bar{B} \rightarrow D^{(*)}\tau\bar{\nu}$ ”. In: *Phys. Rev. D* 88 (9 Nov. 2013), p. 094012. DOI: 10.1103/PhysRevD.88.094012. URL: <https://link.aps.org/doi/10.1103/PhysRevD.88.094012>.
- [56] R. Alonso, B. Grinstein, and J. Martin Camalich. “ $SU(2) \times U(1)$ gauge invariance and the shape of new physics in rare B decays”. In: *Phys. Rev. Lett.* 113 (2014), p. 241802. DOI: 10.1103/PhysRevLett.113.241802. arXiv: 1407.7044 [hep-ph].
- [57] D. Straub et al. *flav-io/flavio v0.22.1*. June 2017. URL: <https://doi.org/10.5281/zenodo.821015> (visited on 04/16/2018).
- [58] J. Aebischer et al. “WCxf: an exchange format for Wilson coefficients beyond the Standard Model”. In: (2017). arXiv: 1712.05298 [hep-ph].
- [59] M. Misiak et al. “Estimate of $\mathcal{B}(\bar{B} \rightarrow X_s\gamma)$ at $O(\alpha_s^2)$ ”. In: *Phys. Rev. Lett.* 98 (2 Jan. 2007), p. 022002. DOI: 10.1103/PhysRevLett.98.022002. URL: <https://link.aps.org/doi/10.1103/PhysRevLett.98.022002>.

Bibliography

- [60] M. Misiak and M. Steinhauser. “NNLO QCD corrections to the $B^- \rightarrow X_s \gamma$ matrix elements using interpolation in m_c ”. In: *Nuclear Physics B* 764.1 (2007), pp. 62–82. ISSN: 0550-3213. DOI: <https://doi.org/10.1016/j.nuclphysb.2006.11.027>. URL: <http://www.sciencedirect.com/science/article/pii/S055032130600962X>.
- [61] C. Bobeth et al. “ $B_{s,d} \rightarrow \ell^+ \ell^-$ in the Standard Model with Reduced Theoretical Uncertainty”. In: *Phys. Rev. Lett.* 112 (10 Mar. 2014), p. 101801. DOI: 10.1103/PhysRevLett.112.101801. URL: <https://link.aps.org/doi/10.1103/PhysRevLett.112.101801>.
- [62] C. Itzykson and J.-B. Zuber. *Quantum field theory*. 2. print., internat. student ed. International series in pure and applied physics. New York: McGraw-Hill, 1986. ISBN: 0070320713.
- [63] M. Fierz. “Zur Fermischen Theorie des β -Zerfalls”. In: *Zeitschrift für Physik* 104.7 (July 1937), pp. 553–565. ISSN: 0044-3328. DOI: 10.1007/BF01330070. URL: <https://doi.org/10.1007/BF01330070>.
- [64] J. F. Nieves and P. B. Pal. “Generalized Fierz identities”. In: *Am. J. Phys.* 72 (2004), pp. 1100–1108. DOI: 10.1119/1.1757445. arXiv: hep-ph/0306087 [hep-ph].

Eigenständigkeitserklärung

Hiermit versichere ich, dass ich diese Arbeit selbstständig verfasst, keine anderen als die angegebenen Quellen und Hilfsmittel benutzt und die Arbeit bisher oder gleichzeitig keiner anderen Prüfungsbehörde vorgelegt habe.

Würzburg, den 6.6.2018

Peter Meinzing